Rev. Adv. Mater. Sci. 30 (2012) 201-224

REVIEW ON GRAIN BOUNDARIES IN GRAPHENE. CURVED POLY- AND NANOCRYSTALLINE GRAPHENE STRUCTURES AS NEW CARBON ALLOTROPES

I.A. Ovid'ko[1,2]

[1]Institute of Problems of Mechanical Engineering, Russian Academy of Sciences, Bolshoj 61, Vasilievskii Ostrov, St. Petersburg 199178, Russia
[2] Department of Mathematics and Mechanics, St. Petersburg State University, St. Petersburg 198504, Russia

Received: October 3, 2011

Abstract. This article briefly summarizes the information now available, from recent experiments, computer simulations and theoretical models, addressing grain boundaries (GBs) in graphene. Special attention is devoted to the structures of GBs in hexagonal crystal lattice of graphene and their description in terms of such point defects as topological dislocations, pentagon-heptagon pairs. Papers are reviewed which deal with both energy characteristics of GBs in graphene and effects of GBs on its mechanical and transport properties. Geometric features of conventional curved carbon allotropes (fullerenes, cones, carbon nanotubes, etc.) and difference in structure between such allotropes and graphene are discussed in terms of topological disclinations (pentagons, heptagons). Also, it is suggested that the presence of GBs with specific defect configurations in graphene can cause formation of its new curved structures that can be treated as new carbon allotropes. Finally, important unsolved problems in fundamental science and applied research of GBs in graphene are outlined.

1. INTRODUCTION

Graphene, a two-dimensional (2D) sheet of covalently bonded carbon atoms, represents a new generation of advanced materials whose potential to transform so many technologies is almost without precedent; see, e.g., [1-4]. In particular, graphene exhibits the outstanding transport properties due to its 2D hexagonal crystal structure and the presence of charge carriers behaving like massless particles [2-5]. In addition, graphene shows superior (highest ever measured) strength desired for a wide range of technologies [3,6]. As a corollary, since its discovery in 2004 [1], graphene with its unique electronic and mechanical properties has attracted an explosively growing attention from both fundamental and applied viewpoints. Studies of graphene are typically focused on its small specimens consisting of single 2D crystallites or, in other terms, single crystalline monolayer graphene. Recently, however, large-area polycrystalline graphene sheets have become the subject of intense research efforts motivated by technological needs; see, e.g., [7-10]. GBs serve as intrinsic structural elements in polycrystalline graphene whose mechanical and functional characteristics are highly sensitive to the presence of GBs; see, e.g., [11-15]. In this context, it is important to understand and describe GBs and their effects on unique electronic and mechanical properties of graphene. Though studies in this area are in their infancy, several intriguing results and remarkable trends have been reported serving as a basis for further progress. The main aim of this paper is to give a brief overview of recent experiments, computer simulations and theoretical models, ad-

Corresponding author: I.A. Ovid'ko, e-mail: ovidko@nano.ipme.ru

© 2012 Advanced Study Center Co. Ltd.

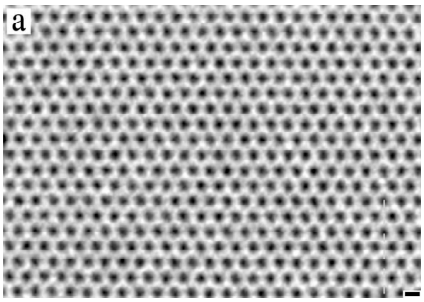

Fig. 1. Direct image of a single-layer graphene membrane (atoms appear white) (for details, see [16]). Reprinted with permission from [J.C. Meyer, C. Kisielowski, R. Erni, M.D. Rossell, M.F. Gommie and A. Zettl, Direct imaging of lattice atoms and topological defects in graphene membranes, *Nano Letters*, Volume 8**,** No 11 (2008) 3582-3586]. Copyright (2008) American Chemical Society.

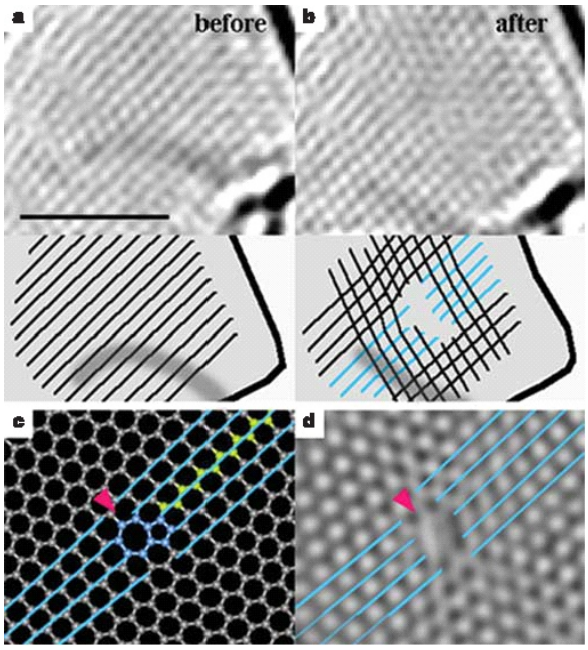

Fig. 2. *In situ* observation of a topological defect induced in a graphene layer. (a), (b) High resolution transmission electron microscopy (HRTEM) images of a single graphene layer with a topological defect induced by electron irradiation (before (a) and after (b)). An edge dislocation is unambiguously visible at the middle of the network where one zig-zag chain is missing through. The missing zig-zag chain is shown schematically in the bottom part of each panel. (c) An atomic model of the pentagon-heptagon pair in the graphitic network. (c) A simulated HRTEM image shows a comparison with the HRTEM image shown in (b). Scale bar, 2 nm (for details, see [17]). Reprinted with permission from [A. Hashimoto, K. Suenaga, A. Gloter, K. Urita and S. Iijima, *Nature,* Volume 430 (2004) 870-873.]. Copyright (2004) by the Nature Publishing Group.

dressing GBs and their effects on transport and deformation processes in graphene. Also, in this paper, it will be suggested that the presence of GBs with specific defect configurations in graphene can cause formation of its new curved structures that can be treated as new carbon allotropes. Finally, important unsolved problems in fundamental science and applied research of GBs in graphene – in particular, questions related to tuning of its electron transport and mechanical properties through GB engineering – will be outlined.

2. GRAIN BOUNDARY STRUCTURES IN GRAPHENE. THEORY AND COMPUTER SIMULATIONS

Pristine graphene structures represent 2D plane sheets of covalently bonded carbon atoms that form ideal hexagonal crystal lattices (Fig. 1). Typical defects experimentally observed in graphene are vacancies [16,17], Stone-Wales defects [16], edges [16,18] , dislocations (Fig. 2) (see also models of dislocations in the hexagonal lattice [19] in Figs. 3a, 3b, and 3c) and GBs [11-15] (Fig. 4) (see also models of GBs in the hexagonal lattice [19] in Figs. 3d and 3e).

Graphene specimens exist as either monolayers attached to substrates made of another material (mostly SiC or a metal) or free-standing sheets/membranes. Following [3], the term "free-standing graphene" means that a graphene membrane is sufficiently isolated from its environment. In the case of graphene-substrate systems, defects in graphene monolayers may be influenced by pre-existent defects on substrate surfaces. In the case of free-standing graphene sheets, buckling of such sheets can occur due to elastic strains created by defects; see, e.g., [19,20] (Fig. 3f).

GBs are line defects separating graphene grains (crystallites/domains) with different crystal lattice orientations (Figs. 3d and 3e; and 4). GBs in 2D graphene sheet are tilt boundaries characterized by tilt misorientation angles θ, that is, angles specifying misorientation between adjacent crystal lattices. More precisely, a tilt boundary in a graphene monolayer by definition separates two 2D grains whose crystal lattices are rotated relative each other by a tilt misorientation angle θ (characterizing the boundary), with the rotation axis being perpendicular to the monolayer plane. A tilt boundary is called symmetric, if misorientations, θ_1 and θ_2, of crystal lat-

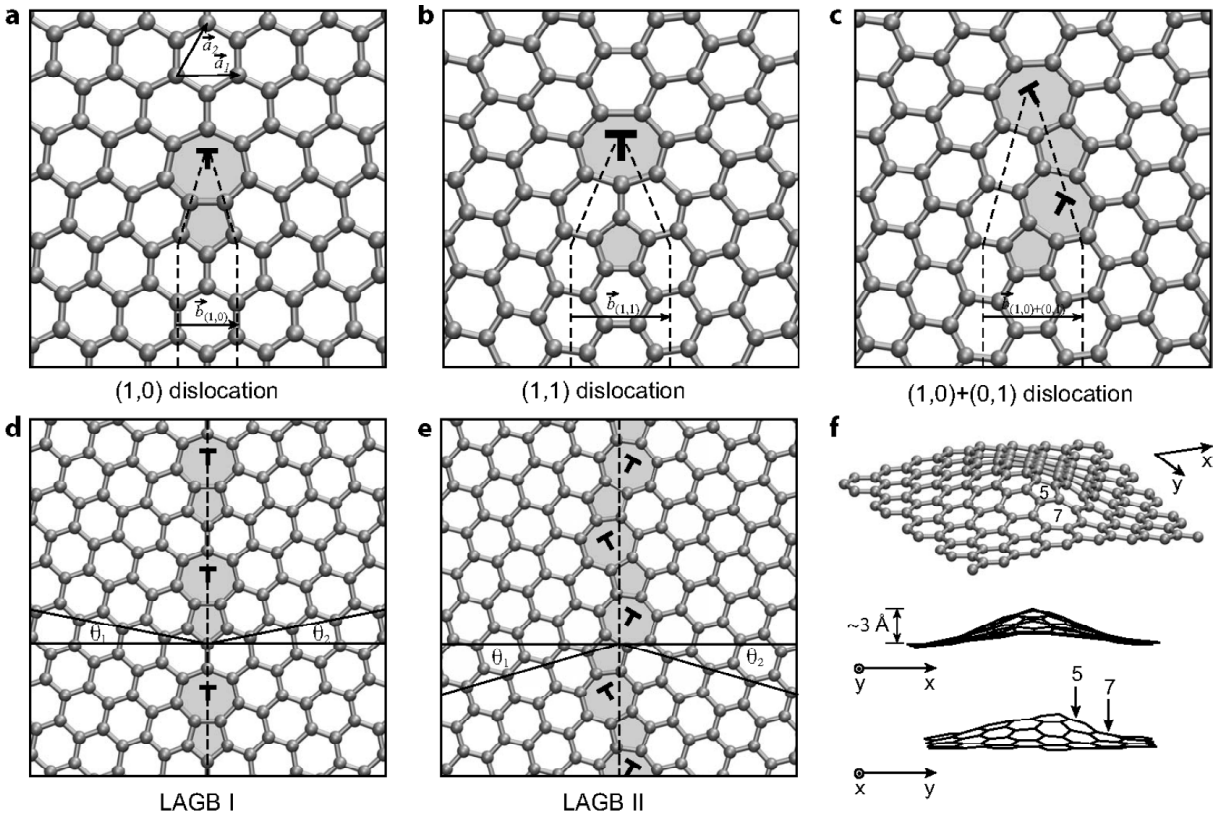

Fig. 3. (a)-(c) Atomic structures of (1,0)- and (0,1)-dislocations, and a (1,0)- and (0,1)-dislocation pair, respectively (for details, see [19] and text). The dashed lines delimit the introduced semi-infinite strips of graphene originating at the dislocation core. Non-six-membered rings are shaded. (d) and (e) Atomic structures of the $\theta = 21.8^{o}$ (LAGBI) and the $\theta = 32.2^{o}$ (LAGBII) symmetric large-angle grain boundaries, respectively. The dashed lines show the boundary lines and the solid lines definite angles θ_1 and θ_2. (f) Buckling of the graphene layer due to the presence of a (1,0)–dislocation (for details, see [19]). Reprinted with permission from [O.V. Yazyev and S. Louie, *Physical Review B,* Volume 81 (2010) article 195420.], Copyright (2010) by the American Physical Society.

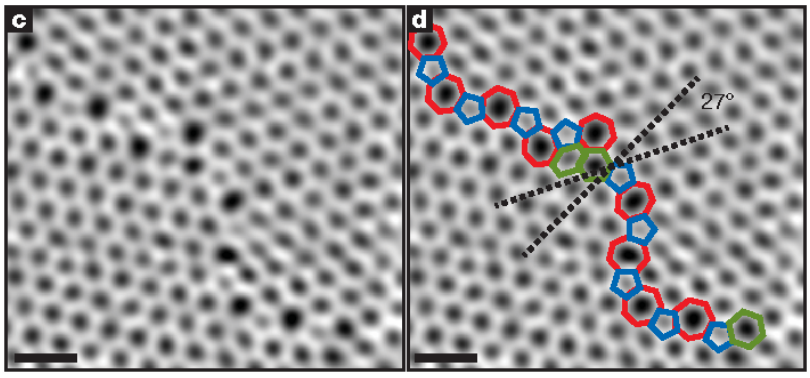

Fig. 4. Atomic-resolution ADF-STEM images of graphene crystals. (a) Two grains (bottom left, top right) intersect with a 27° relative rotation. An aperiodic line of defects stitches the two grains together. (b) The image from (a) with the pentagons (blue) and distorted hexagons (green) of the grain boundary outlined. (a),(b) were low-pass-filtered to remove noise; scale bar, 5 Å (for details, see [11]). Reprinted with permission from [P. Y. Huang, C.S. Ruiz-Vargas, A. M. van der Zande, W.S. Whitney, M.P. Levendorf, J.W. Kevek, S. Garg, J.S. Alden, C.J. Hustedt, Y. Zhu, J. Park, P.L. McEuen and D.A. Muller, *Nature,* Volume 469 (2011) 389-393]. Copyright (2011) by the Macmillan Publishers Limited.

tices of its adjacent grains relative to the normal of the boundary line are the same [19,20]. That is, $\theta_1 = \theta_2$, where $\theta_1 + \theta_2 = \theta$; see examples in (Fig. 3d and 3e). Asymmetric tilt boundaries are specified

by the non-zero inclination angle, θ_1-θ_2, showing deviation of the tilt boundary from its symmetric configuration [19,20]. Asymmetric tilt boundaries produce long-range stress fields and thereby are characterized by large elastic energies. As a corollary, asymmetric tilt boundaries tend to be located in the only vicinities of either other stress sources or graphene sheet edges which effectively screen the stress fields of these boundaries.

In this paper, we will focus our consideration on the structural features of symmetric tilt boundaries as most widespread GBs in graphene. A systematic description of symmetric tilt boundaries in graphene in terms of perfect topological dislocations has been recently done in papers [19,20]. In the framework of this approach having its roots in the dislocation model [21] of GBs in graphite, low- and high-angle tilt boundaries in graphene are represented as walls of topological edge dislocations. Before discussion of GB structures in terms of dislocations, let us consider, following [19], typical configurations of perfect topological dislocations in graphene. Such dislocations are specified by their Burgers vectors and dislocation core structures (Fig. 3a, 3b, and 3c). The Burgers vectors $\boldsymbol{b}$ of perfect dislocations are lattice vectors of a 2D hexagonal crystal having basic vectors $\boldsymbol{a}_1$ and $\boldsymbol{a}_2$. In doing so, any Burgers vector is given by the expression: $\boldsymbol{b} = m\boldsymbol{a}_1 + n\boldsymbol{a}_2$, where integers, m and n, unambiguously specify geometry of the corresponding dislocation.

Yazyev and Louie [19] distinguished the following three classes of topological dislocation configurations serving as typical structural blocks of GBs in graphene: (1,0)–dislocations (Fig. 3a), (1,1)-dislocations (Fig. 3b) and pairs of (1,0)- and (0,1)-dislocations (Fig. 3c). The (1,0)–dislocation core contains edge-sharing heptagon-pentagon pair called also the armchair configuration (Fig. 3a). The (1,1) – dislocation core consists of heptagon and pentagon separated by carbon-carbon bond (Fig. 3b). A pair of (1,0)- and (0,1)-dislocations is characterized by the sum Burgers vector (1,1) and has a zigzag core configuration consisting of two heptagon-pentagon pairs, as it is shown in Fig. 3c.

Note that pentagons and heptagons serve as topological disclinations - point defects associated with rotational symmetry - in hexagonal crystal lattice of graphene. In this context, perfect dislocations in graphene are treated as disclination dipoles, pairs of positive and negative topological disclinations being pentagons and heptagons, respectively (Figs. 3a, 3b, and 3c). We will discuss disclinations in graphene and other carbon nanostructures in more detail in Sections 5 and 6.

In the framework of the approach [19] based on geometry of hexagonal crystal lattices, symmetric tilt boundaries with misorientation angles θ being in the range from 0^o to 60^o in graphene are represented as periodic walls of (1,0)–dislocations (if θ ranges from 0^o to 28.1^o) and walls of either (1,1)-dislocations or pairs of (1,0)- and (0,1)-dislocations (for θ being in the range from 28.1^o to 60^o); see, e.g., Figs. 3d and 3e. The GB misorientation interval from 0^o to 60^o is chosen, because a 2D hexagonal lattice is symmetric relative to in-plane rotation by $k\pi/3$ (or, in other terms, $k(60^o)$), with k being an integer.

In general, different dislocation configurations can compose GBs with the same misorientation parameters. Besides, structural motifs of a GB in graphene are sensitive to orientation of its lines relative to hexagons of its adjacent grain lattices. In this situation, selection of dislocations as structural blocks of GBs in graphene can be effectively done by analysis of their energy characteristics, but not only their geometric aspects. Results of GB energy consideration based on computer simulations of graphene bi-crystal structures were presented in papers [19,20]. Although these computer simulations show pictures different in details, their key trends are similar.

First, let us discuss results of computer simulations [20] concerning the energy characteristics and structural features of periodic symmetric GBs in graphene. Liu and Yakobson [20] examined GB structures in graphene in the two cases: flat graphene (say, graphene having a strong binding to a flat substrate) and free-standing graphene where elastic strains of GB dislocations can produce local buckling. In both cases, regular walls of (1,0)–dislocations are found to be structural blocks composing symmetric tilt boundaries with tilt misorientation angle θ ranging from 0^o to 21.8^o (Fig. 5). (In doing so, when the GB misorientation angle θ is close to 0^o, GBs have their lines nearly perpendicular to edges shared by heptagons and pentagons of (1,0)–dislocations (Fig. 5).) The GB dislocation density increases from 0 to its maximum value (Fig. 5c) when θ rises from 0^o to 21.8^o.

In the range of tilt misorientation angle θ from 21.8^o to 60^o, the low-energy GB structures consist of (1,1)-dislocations in a strictly flat graphene [20] (Fig. 5). The GB dislocation density increases from some value (corresponding to the transition from the (1,0)–dislocation structure to the (1,1)–dislocation structure) to its maximum value (Fig. 5d) when θ rises from 21.8^o to 32.2^o. The GB dislocation density decreases from its maximum value to 0 when θ rises from 32.2^o to 60^o [20] (Fig. 5).

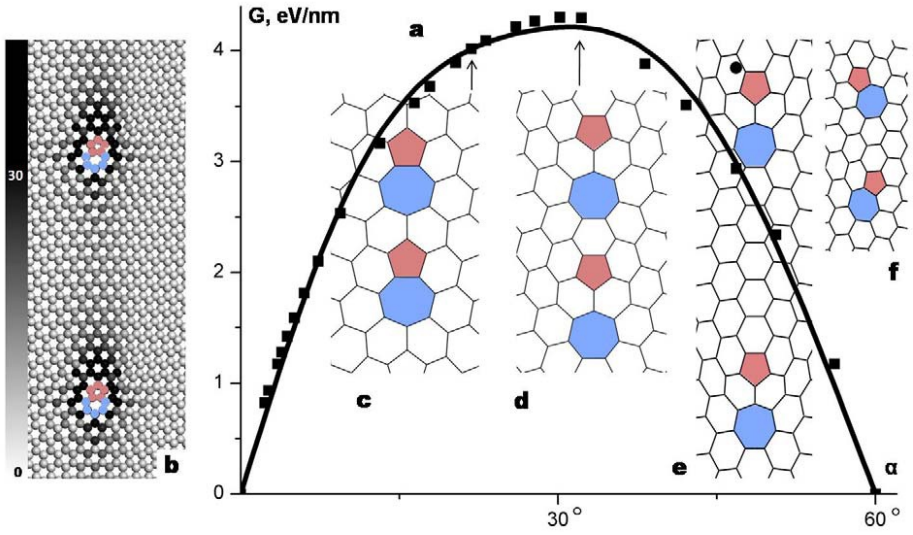

Fig. 5. (a) Grain boundary energies $G(\alpha)$ as a function of tilt angle α (in the main text, this angle is designated by θ), based on 26 computed data points (solid squares) and fitted by the three-terms of Fourier series (thick line). (b) Nearly arm-chair interface low-angle grain boundary ($\alpha = 3.5^o$) with gray-level coded strain energy per atom, shown in meV. (c) Grain boundary with maximum density of (1,0)–dislocations, $\alpha = 21.8^o$. (d) Grain boundary with maximum density of (1,1)–dislocations, $\alpha = 32.2^o$. (e) Nearly zig-zag interface low-angle grain boundary (α - $60^o = 13.2^o$) comprised of (1,1)–dislocations and (f) its alternative split into slanted (1,0)- and (0,1)-dislocations, higher in energy (solid circle) (for details, see [20]). Reprinted with permission from [Y. Liu and B.I. Yakobson, Cones, pringles, and grain boundary landscapes in graphene topology, *Nano Letters*, Volume 10**,** No 6 (2011) 2178-2183]. Copyright (2011) American Chemical Society.

In the situation with free-standing graphene, its buckling in the third dimension comes into play, and this factor allows an exchange of in-plane elastic energy for bending energy. In particular, due to buckling, the elastic energy of GBs in some ranges of tilt misorientation parameter θ is lowered by splitting (1,1)-dislocations into pairs of (1,0)- and (0,1)-dislocations [20] (Fig. 5).

In computer simulations [19], the splitting process in question was found to be preferred in even strictly flat graphene, for GBs with the tilt misorientation angle θ being in the range from 21.8^o to 60^o. Also, as with the approach [20], the energy analysis [19] showed that lowest-energy tilt boundaries with the misorientation angle θ ranging from 0^o to 21.8^o represent periodic walls of (1,0)–dislocations. As a corollary, following computer simulations [19], dislocations with shortest Burgers vectors are sufficient for constructing the most stable GB structures at any given misorientation angle θ from 0^o to 60^o in flat graphene. Besides, it was found that buckling effectively reduces the GB energies in free-standing graphene, while the structural blocks – dislocations - of lowest-energy GBs are the same as with flat graphene [19].

On the basis of their computer simulations, Yazyev and Louie [19] revealed that, the energy of low-angle GBs (specified by the misorientation angles in the intervals $\theta < 10^o$ and $60^o - \theta < 10^o$) is well approximated by the Read-Shockley expression:

$$E(\theta') = \frac{Gb\theta'\left[1 + \ln\left(b / 2\pi r_0\right) - \ln\theta'\right]}{4\pi\left(1-\nu\right)}. \qquad (1)$$

Here G denotes the shear modulus, b the Burgers vector modulus, ν the Poisson ratio, and r_o the dislocation core radius (estimated as 0.96 Å). Note that the Read-Shockley expression also effectively describes the energies of low-angle GBs in conventional three-dimensional (3D) crystals; see, e.g., [22,23]. In this context, there is a certain similarity in trends exhibited by the energy characteristics of low-angle GBs in graphene and conventional 3D crystals.

The discussed theoretical and computer models [19,20] operate with periodic and straight symmetric tilt boundaries. At the same time, experimentally observed GB structures (see Section 3) are in some respects different from the discussed periodic and straight symmetric structures (Figs. 3e and 3f; Fig. 5). Nevertheless, the dislocation representations [19,20] of GBs serve as an effective approximate basis for analysis of real GBs in graphene.

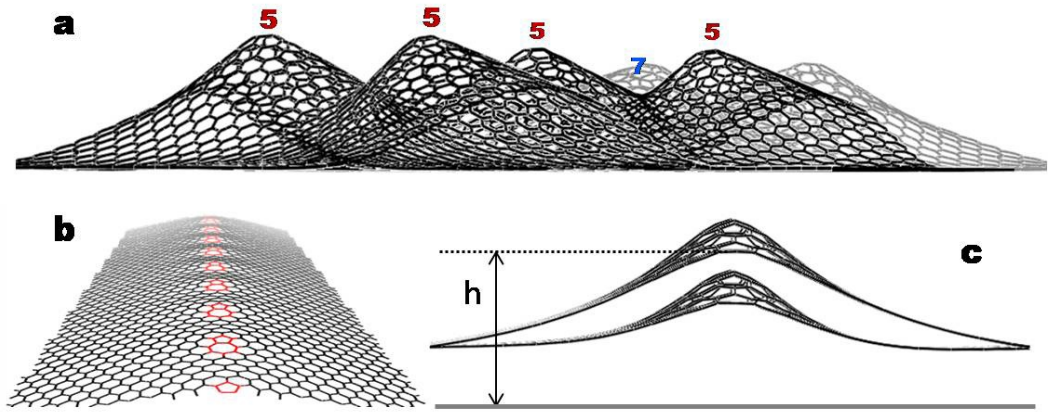

Fig. 6. (a) A computed (full energy relaxation) landscape due to presence of scattered pentagons and heptagons – disclination defects - in a perfect graphene lattice, shows elevation roughly equal to the distances between the pentagons and heptagons. (b) A regular grain boundary from (1,0)–dislocations forms a ridge shape. (c) Flattening effect of the van der Waals attraction to the substrate, as compared for the two values 4V and V, when the elevation $h - h_{flat}$ approximately doubles (for details, see [20]). Reprinted with permission from [Y. Liu and B.I. Yakobson, Cones, pringles, and grain boundary landscapes in graphene topology, *Nano Letters*, Volume 10**,** No 6 (2011) 2178-2183]. Copyright (2011) American Chemical Society.

Finally, in this section, let us briefly discuss the buckling effect induced by scattered pentagons and heptagons in graphene. This effect in a first approximation may illustrate the buckling effect produced by disordered GBs in free-standing graphene sheets. Following Liu and Yakobson [20], a rather pronounced 3D landscape with peaks and valleys forms in graphene due to scattered pentagons and heptagons whose numbers are supposed to be equal (Fig. 6a). In doing so, distortions created by a pentagon-heptagon pair - a topological dislocation - are specified by the buckling height which is close to the distance $h_{5\text{-}7}$ between its constituent pentagon and heptagon. Arrangement of pentagon-heptagon pairs into a periodic line GB causes formation of linear bridges in a graphene sheet [20] (Fig. 6b) in agreement with experimental data [24].

If a graphene monolayer with a 3D landscape created by pentagon-heptagon pairs is attached to a substrate, the landscape is partially flattened owing to the interaction between atoms of the graphene sheet and the substrate, the namely van der Waals attraction specified by the energy V per unit area. This effect of the substrate is illustrated in Fig. 6c showing two landscapes with different values of the attraction energy [20].

3. EXPERIMENTAL OBSERVATIONS OF GRAIN BOUNDARIES IN GRAPHENE

Now let us consider experimental observations of GBs in graphene. In general, real GBs in graphene are different from their idealized, straight and periodic, models exploited in theoretical examinations and computer simulations. In most cases, experimentally observed GBs in graphene are not straight and show no strict periodicity.

For instance, Huang *et al.* [11] observed and characterized (by transmission electron microscopy (TEM) and annular dark-field scanning electron microscopy (ADF SEM) techniques) a tilt GB boundary with tilt misorientation angle = 27° in a graphene monolayer (Fig. 4). It was experimentally found that the GB consists of pentagon-heptagon pairs (or, in other terms, topological dislocations) and distorted hexagons. This picture is well consistent with theoretical and computer models of GBs in graphene (see section 2). For instance, in the GB structure presented in Fig. 4, one can distinguish (1,0)– and (1,1)-dislocations as well as pairs of (1,0)- and (0,1)-dislocations.

At the same time, the experimentally observed GB (Fig. 4) is not straight, and its dislocation structure is not periodic. That is, this GB does not belong to typical classes of GB dislocation walls (Figs. 3d and 3e as well as Fig. 5) revealed in the energy minimization analysis based on computer simulations [19,20].

Kim *et al.* [13] experimentally observed tilt boundary with misorientation = 26.6° in a graphene monolayer (Fig. 7). Its characterization with the aid of TEM and ADF SEM methods revealed curved and non-periodic GB structure consisting of pentagon-heptagon pairs (topological dislocations) and distorted hexagons. As with the previously discussed

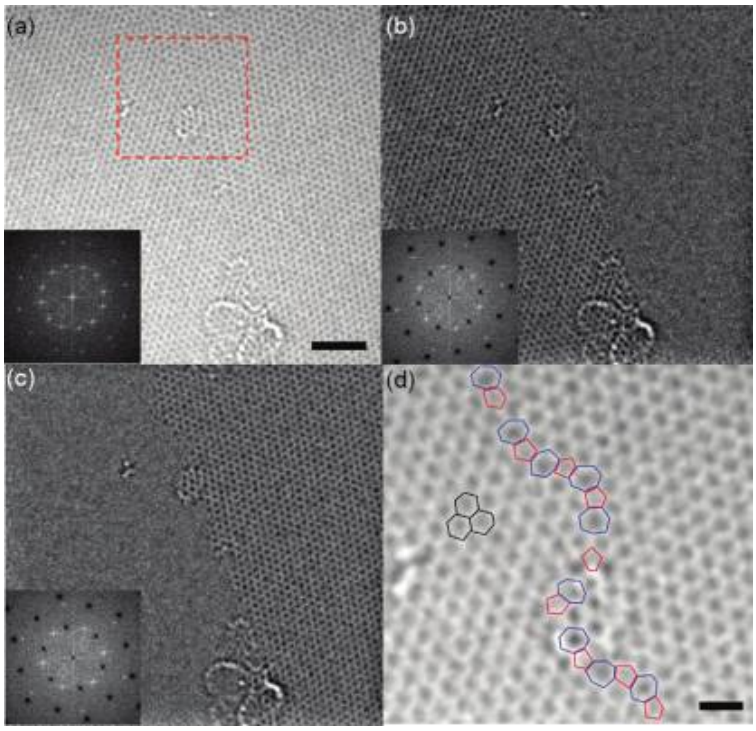

Fig. 7. Atomic-resolution images of a high-angle tilt grain boundary of graphene. (a) Atomic-resolution image of graphene grain boundary. The left and right parts of the image are different tilt grains, which are relatively tilted by 26.6°. The red dashed rectangle is the field of view of panel (d). The inset shows the Fourier transform of the image. It shows the two sets of hexagonal patterns from two grains. The scale bar is 2 nm. (b) Atomic-resolution image of the same region after removing one set of hexagonal patterns from the fast Fourier transform. The contrast of the right side of the image completely disappears, indicating that the graphene has no defects inside the right side grain. (c) Atomic-resolution image after removing another set of hexagonal patterns from the fast Fourier transform. The left side of the image disappears. (d) Zoom-in image of the high-angle tilt grain boundary of graphene. The pentagon, hexagon and heptagon are overlaid with red, black, and blue polygons, respectively. The grain boundary shows an array of alternating pentagon and heptagon structures. The scale bar is 0.5 nm (for details, see [13]). Reprinted with permission from [K. Kim, Z. Lee, W. Regan, C. Kisielowski, M.F. Gommie and A. Zettl, Grain boundary mapping in polycrystalline graphene, *ACS Nano,* Volume 5, No 3 (2011) 2142-2146]. Copyright (2011) American Chemical Society.

case, (1,0)– and (1,1)-dislocations as well as pairs of (1,0)- and (0,1)-dislocations can be found in the examined GB structure (Fig. 7). The difference between model, low-energy GBs specified by periodicity and straight geometry and real, curved GBs with irregular dislocation structures is logically attributed to non-equilibrium conditions of formation of real GBs in graphene. These conditions produce "kinetically frozen" GBs whose energies exceed minimum values inherent to model GBs.

In parallel with curved GBs, there are examples of loop GBs in graphene. For instance, Cockayne with co-workers [14] simulated and experimentally observed such GBs showing sixfold (C_6) symmetry in epitaxial graphene grown on SiC (Figs. 8 and 9). These loop GBs contain rotating sequences of pentagon-heptagon pairs (topological dislocations), that close on themselves. For illustrative aims, one can represent formation of loop GBs as that resulted from the following imaginary procedure: first, one cuts out a circle-like portion of pristine hexagonal lattice of graphene; then, this portion is rotated relative to the pristine lattice in its plane; and, finally the rotated portion is matched to the pristine lattice, in which case the rotation misfit is accommodated by a corresponding rotating sequence of pentagon-heptagon pairs.

In Fig. 8a, the smallest member of the family of loop GBs with sixfold symmetry in graphene is shown. This configuration is called the flower defect, and the namely this defect was observed in the scanning tunneling microscopy experiment (Fig.

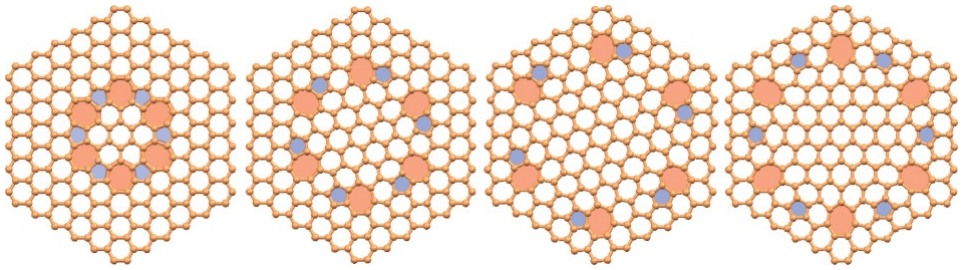

Fig. 8. Schematic structures of the rotational grain boundary family C_6 (*m,n*) with C_6 symmetry in graphene. (a) Structure C_6 (*1,1*). (b) Structure C_6 (*2,1*). (c) Structure C_6 (*3,1*). (d) Structure C_6 (*2,2*). The structure in (a) is the flower defect. Seven- and fivefold rings are colored pink and blue, respectively (for details, see [14]). Reprinted with permission from [E. Cockayne, G.M. Rutter, N.P. Guisinger, J.N. Crain, P.N. First and J.A. Stroscio, *Physical Review B,* Volume 83 (2011) article 195425.], Copyright (2011) by the American Physical Society.

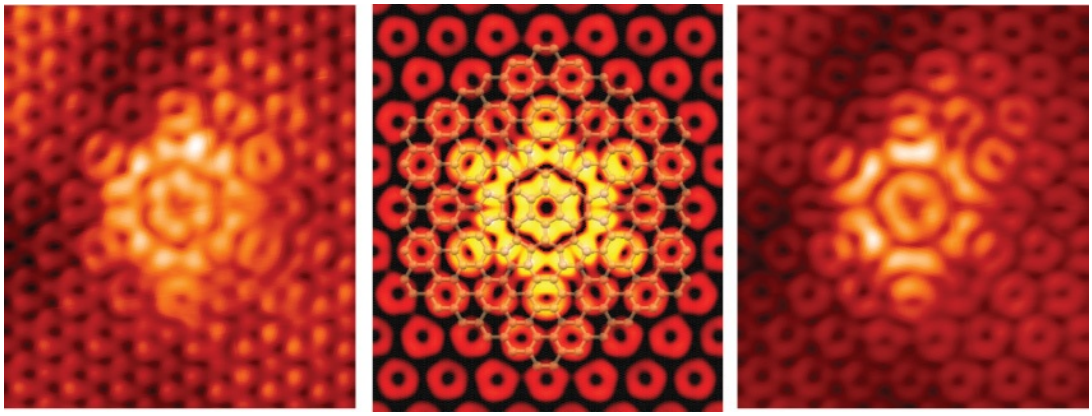

Fig. 9. A comparison of experimental and simulated scanning tunneling microscopy (STM) images of the C_6 (*1,1*) rotational grain boundary. STM topographs of a sixfold defect observed in the growth of epitaxial graphene on SiC at (a) - 300 and (c) 300 mV sample bias. (b) Simulated STM image of the C_6 (*1,1*) rotational grain boundary (for details, see [14]). Reprinted with permission from [E. Cockayne, G.M. Rutter, N.P. Guisinger, J.N. Crain, P.N. First and J.A. Stroscio, *Physical Review B,* Volume 83 (2011) article 195425.], Copyright (2011) by the American Physical Society.

9) [14]. The flower defect and other loop GBs are specified by rather low energies and thereby represent stable defects in graphene [14].

We discussed the specific structural features of GBs consisting of pentagon-heptagon pairs (topological dislocations) and distorted hexagons in graphene, preserving the threefold coordination of the carbon atoms. At the same time, there are also examples where such defects as dangling bonds (violating the threefold coordination of the carbon atoms) are present at GBs. For instance, An *et al.* [25] reported on the existence of dangling bonds at GBs in graphene grown on Cu. That is, GBs can locally contain dangling bonds, instead of pentagons and heptagons. Also, it was observed that GBs and their vicinities in graphene are typically covered by adsorbates, and this is indicative of enhanced absorption ability of GBs [25].

Now let us turn to discussion of GB ensembles and their characteristics in graphene. An et al [25] analyzed a GB misorientation distribution in a polycrystalline graphene grown on Cu. They found a rather interesting asymmetry in the GB misorientation distribution, the namely dominance of high-angle boundaries having the misorientation angle in the range from 10^o to 30^o. Note that, with the sixfold symmetry of pristine hexagonal lattice, the diffractive imaging technique determines GB misorientation angles θ and 60^o-θ (where $\theta < 60^o$) as the same. That is, all the misorientation angles are given in the range from 0^o to 30^o.

In experiments [11,13] dealing with GB misorientation distributions in free-standing graphene specimens, it was found that GB misorientation angles tend to have more populations around 0^o and 30^o than middle-range angles (Figs. 10 and 11). The difference in grain size distribution between graphene monolayer grown on Cu [25] and free-standing graphene specimens (Figs. 10 and 11) [11,13] can be logically attributed to the important role of local

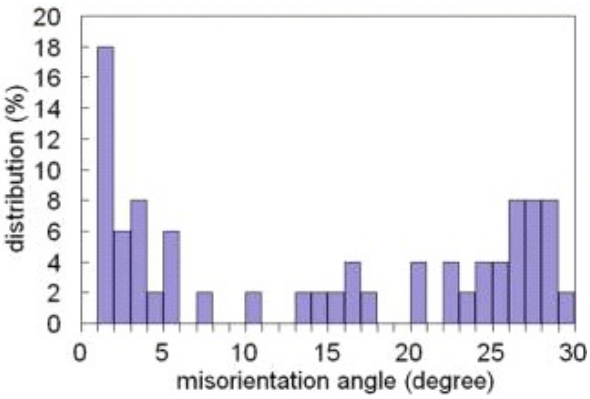

Fig. 10. Distribution of misorientation angles between adjacent grains in graphene. Fifty misorientation angles are measured from rotational angles between two sets of hexagonal diffraction patterns. There are more populations around 0° and 30° than middle-range angles (for details, see [13]). Reprinted with permission from [K. Kim, Z. Lee, W. Regan, C. Kisielowski, M.F. Gommie and A. Zettl, Grain boundary mapping in polycrystalline graphene, *ACS Nano,* Volume 5, No 3 (2011) 2142-2146]. Copyright (2011) American Chemical Society.

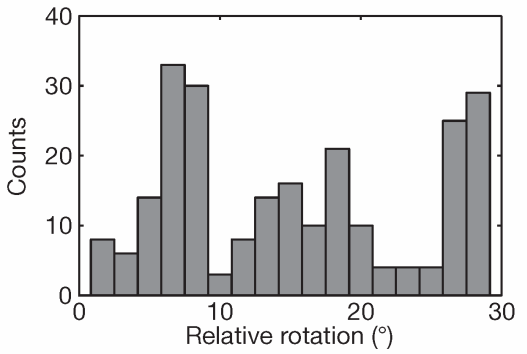

Fig. 11. Histogram of relative grain rotation angles measured from 238 grain boundaries in graphene (for details, see [11]). Reprinted with permission from [P. Y. Huang, C.S. Ruiz-Vargas, A. M. van der Zande, W.S. Whitney, M.P. Levendorf, J.W. Kevek, S. Garg, J.S. Alden, C.J. Hustedt, Y. Zhu, J. Park, P.L. McEuen and D.A. Muller, *Nature,* Volume 469 (2011) 389-393]. Copyright (2011) by the Macmillan Publishers Limited.

buckling processes in relaxation of GB dislocation stresses in free-standing specimens. In such specimens characterized by grain sizes in the range 3 – 10 μm [13] and the mean grain size of around 250 nm [11], the elastic energy of low-angle GBs consisting of topological dislocations arranged with a large dislocation-dislocation interspacing is effectively reduced by local buckling in the third dimension. In contrast, polycrystalline graphene monolayer attached to Cu film [25] and specified by comparatively large grain sizes > 10 μm can not show pronounced local buckling. Therefore, low-angle GBs characterized by misorientation angles $\theta \geq 10^{o}$ and comparatively large elastic strain energies (due to comparatively large dislocation-dislocation interspacing) are not favorable in flat graphene.

GBs in few-layer graphene grown on SiC have been examined in experiments [12]. Few-layer graphene attached to a substrate has some specific structural features which differentiate it from conventional graphene monolayer. In particular, a moire' superplattice can be formed on a few-layer graphene due to mutual rotation of its layers [12]. In this situation, interfaces between mutually rotated graphene layers may be treated as twist boundaries. Biedermann with co-workers [12] observed two morphologies of few-layer graphene in their experiments: smooth (atomically flat) and rough morphologies. The rough graphene is specified by rms roughness of typically 0.15-0.20 nm and contains unusually wide GB regions (Fig. 12). In Fig. 12, such a GB region is shown which separates large misoriented grains, has the width of ~ 50 nm and contains randomly oriented parallel 1D features with a periodicity of ~ 4 nm. This wide GB structure is unusual and, in a first approximation, may be treated as a kind of the nanocrystalline graphene structure separating large misoriented grains/crystallites of graphene.

4. EFFECTS OF GRAIN BOUNDARIES ON MECHANICAL AND TRANSPORT PROPERTIES OF GRAPHENE

Conventional GBs in 3D polycrystalline and nanocrystalline solids significantly or even crucially influence their mechanical, physical and chemical properties; see, e.g., [26-31]. In this context, it is logical to expect that line GBs cause dramatic effects on the properties of 2D graphene. This view is convincingly supported by experimental data, computer simulations and theoretical studies which will be discussed below.

In general, the effects of GBs on the properties of graphene can be divided into the following four categories: (i) the effects of GB dislocation cores (pentagon-heptagon pairs); (ii) the effects associated with orientation mismatch between grains/crystallites matched at GBs; (iii) the effects of in-plane strains induced by GBs; and (iv) the effects of local

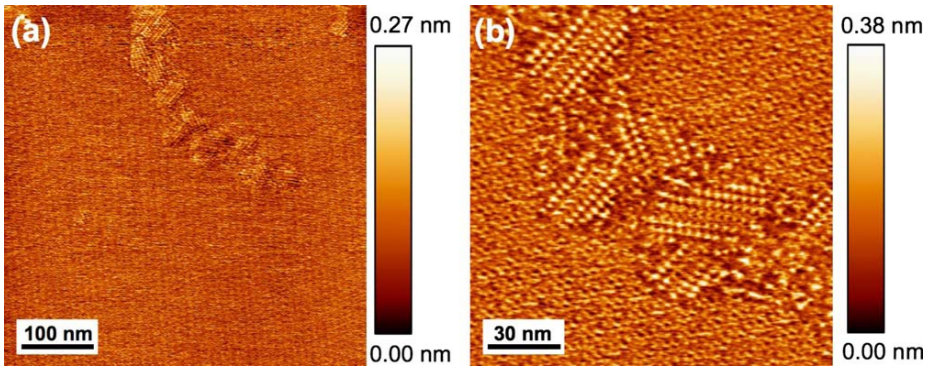

Fig. 12. Scanning tunneling microscopy images of a region from the graphene grown at 1500 °C. In (a), a 500 x 500 nm^2 image showing the presence of a grain boundary in the upper half of the image. In (b), a 150 x 150 nm^2 image showing the parallel 1D features within the grain boundary. Scan parameters are I_{set} = 2 nA and V_{bias} = 100 mV for (a) and (b) (for details, see [12]). Reprinted with permission from [L.B. Biedermann, M.L. Bolen, M.A. Capano, D. Zemlyanov, R.G. Reifenberger, *Physical Review B,* Volume 79 (2009) article 125411.], Copyright (2009) by the American Physical Society.

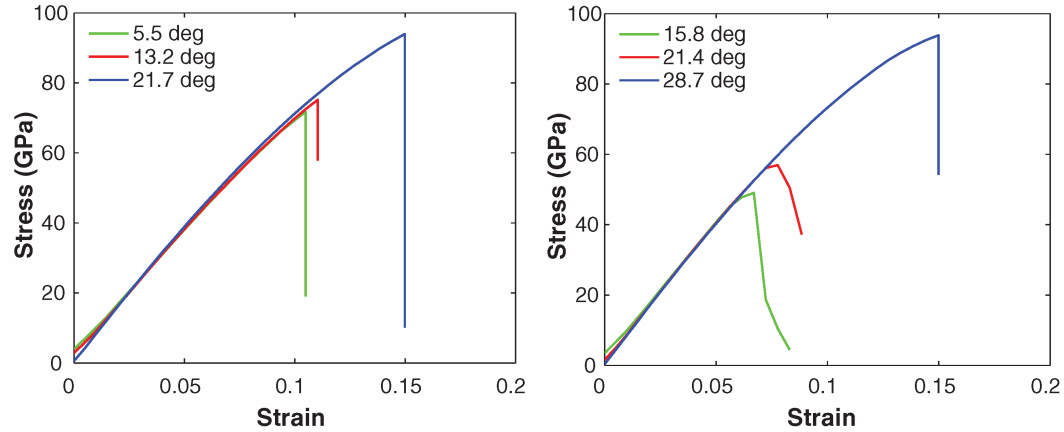

Fig. 13. The stress-strain curves of (**left**) zigzag-oriented and (**right**) armchair-oriented graphene sheets pulled perpendicular to the grain boundaries (for details, see [32]). Reprinted with permission from [R. Grantab, V.B. Shenoy and R.S. Ruoff, *Science,* Volume 330 (2010) 946-948]. Copyright (2010) by the American Association for the Advancement of Science.

buckling induced by GBs. These effects on a given property can range rather widely, depending on the property, polycrystalline graphene structure and external conditions.

First, let us discuss the mechanical properties of graphene with GBs. Following experimental data [11], the failure strength of free-standing polycrystalline graphene under concentrated mechanical load dramatically degrades compared to single-crystal graphene membranes. In this experiment, a polycrystalline graphene membrane was loaded by tip of atomic force microscope. It was found that the graphene tears along GBs at load of ~100 nN [11]. This value is an order of magnitude lower than typical values (~1.7 μN) specifying fracture of single-crystal exfoliated graphene [6].

Strength characteristics of graphene bi-crystals with tilt GBs have been examined in computer simulations [32]. The key focuses were placed on sensitivity of the strength to GB misorientation depending on the GB dislocation structure. The tests in these computer simulations were performed with graphene sheets pulled perpendicular and parallel to GB lines. For the load geometries in question, computer simulations [32] show the trend that, as the GB misorientation increases, both the ultimate failure strength and strain at failure grow. In particular, it was found that graphene sheets containing high-angle GBs (specified by misorientatioin angles close to 20° - 30°) with dense dislocation structures have strength values exceeding those of graphene sheets containing low-angle GBs with low-density dislocation structures [32] (Fig. 13).

Grantab with co-workers [32] interpreted their non-intuitive results in terms of critical carbon-carbon bonds revealed in computer simulations as

bonds whose breaks represent the critical starting events for complete failure of graphene sheets. In the framework of the discussed interpretation, initial local strains created by low-density dislocation structures of low-angle GBs in graphene before its mechanical load are higher than those created by high-density dislocation configurations composing high-angle GBs. (This statement follows from the standard theory of dislocation walls in solids [23].) That is, initial strains at critical bonds in the case of low-angle boundaries are high enough to initiate failure at lower level of the applied external stress, compared to the case of high-angle GBs.

Now let us discuss the effects of GBs on transport properties of graphene. Huang *et al.* [11] probed electric resistance of GBs in comparison with that of GB-free areas of graphene. They experimentally revealed that the resistance of GBs is less than one third the resistance of 250 nm grain. Thus, following the experimental data [11], the transport properties of graphene degrade due to GBs, but the measured resistance of GBs is not dramatically different (by orders in magnitude) from that of graphene free from GBs. Similar results have been reported by Yu with co-workers [15]. They performed experimental measurements of GB resistance in graphene grown on polycrystalline Cu substrate [15]. They revealed that GBs impede the electrical transport properties, providing "extra" resistance, compared to graphene areas free from GBs. At the same time, this "extra" GB resistance is not dramatically different from intragrain resistance.

Paper [33] presented results of first principle calculations focused on the electronic structure of tilt GBs in graphene. This study based on analysis of three symmetric periodic tilt boundaries with different misorientation angles indicates that the electronic structure exhibits a rather complex evolution towards graphene bulk, as the GB tilt misorientation angle decreases. It was found that the occurrence of a Dirac point along the GB direction represents the robust feature of a polycrystalline graphene sheet [33]. Also, high sensitivity of the electronic structure of graphene to its local curvature associated with the presence of pentagon and heptagons in graphene lattice was theoretically revealed in papers [34,35].

A general theoretical analysis of the electronic transport properties of symmetric and asymmetric tilt boundaries characterized by structural periodicity has been done in paper [36] (see also its discussion given by Kim [37]). In particular, Yazyev and Louie [36] theoretically revealed the two distinct transport behaviors of periodic GBs, depending on their structural and geometric features. The first type is high transparency; and this behavior is exhibited, in particular, by all symmetric GBs and some asymmetric GBs. The second type of the GB transport behavior shown by certain asymmetric GBs with specific geometries represents perfect reflection of charge carriers over remarkably large energy ranges (up to ~1 eV). These theoretical results based on the momentum conservation principle were confirmed by first principle calculations [36]. The results under discussion open new intriguing perspectives in graphene-based electronics through GB engineering [36,37].

5. DISCLINATIONS AND CURVATURE IN CONVENTIONAL CARBON NANOSTRUCTURES

In parallel with flat graphene, such curved carbon structures as nanotubes, fullerenes and cones typically exist in nature. These conventional curved carbon structures are topologically and physically distinct from graphene, and non-local curvature plays the definitive role in their specific structural features and properties. In this context, it is highly interesting to describe the difference in topological structure between graphene and conventional curved carbon structures as well as to understand a potential of GBs in tuning non-local curvature and properties of polycrystalline graphene. The structural difference between graphene and conventional curved carbon structures will be considered in this section. On the basis of this consideration, a potential role of GBs as structural elements that can produce non-local curvature in graphene and even generate new carbon allotropes will be discussed in Section 6.

The pronounced sensitivity of properties exhibited by grapheme to curvature-produced strains in its structure distinctly manifests itself in the giant strain-induced pseudo-magnetic field in graphene nanobubbles [38]. The giant field in question was experimentally detected in highly strained nanobubbles of graphen grown on platinum (Pt) substrate (Fig. 14). Such nanobubbles are formed in the graphene during cooling due to a mismatch in thermal expansion coefficient between lattices of graphene and platinum [38]. Nanobubbles typically have a triangular shape and are 4 to10 nm across and 0.3 to 2 nm tall (Fig. 14). The experiment under discussion is a good example of tuning and controlling the properties of graphene through its curvature engineering.

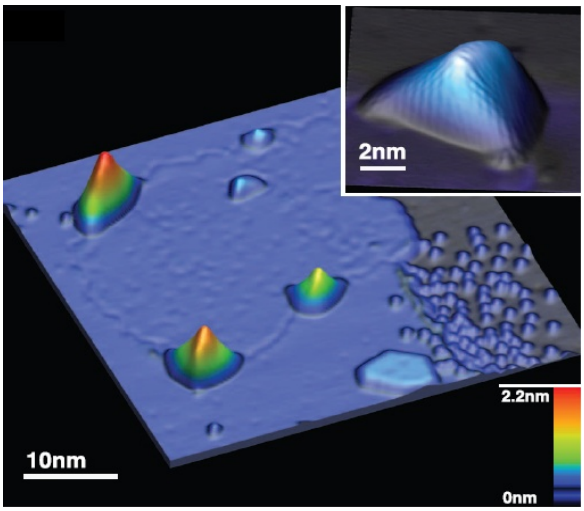

Fig. 14. Scanning tunneling microscopy images of graphene monolayer patch on Pt(111) with four nanobubbles at the graphene-Pt border and one in the patch interior. (Inset) High-resolution image of a graphene nanobubble showing distorted honeycomb lattice resulting from strain in the bubble (for details, see [38]). Reprinted with permission from [N. Levy, S.A. Burke, K.L. Meaker, M. Panlasigui, A. Zettl, F. Guinea, A.H. Castro Neto and M.F. Grommie, *Science,* Volume 329 (2010) 544-547]. Copyright (2010) by the American Association for the Advancement of Science.

In general, manipulations with curvature of graphene (or, in other terms, graphite monolayer) can generate topologically and physically distinct carbon allotropes such as nanotubes, fullerenes, cones and others; see, e.g., [2,39-42]. In doing so, topological disclinations – first of all, pentagons and hexagons – serve as typical carriers of curvature, and their generation in graphene sheets can transform them into conventional curved carbon nanostructures [2, 39-42].

Let us discuss geometry of topological disclinations and their role in formation of curved carbon structures. Pentagons are positive topological disclinations specified by strength = 60° in graphene with hexagonal crystal lattice. Any isolated 60°–disclination (pentagon) in a graphene sheet can be produced by the following imaginary procedure: a cutout of a sheet wedge within an angle 60° from a pristine graphene and subsequent attachment of cut surfaces to each other (Figs. 15a, 15b, and 15c) [39,41]. This procedure preserves the hexagonal crystalline order everywhere in the graphene sheet, except for one elementary cell which becomes a pentagon, a topological 60°–disclination (Fig. 15c).

Disclinations create long-range stresses in graphene sheets. In the case of a free-standing graphene with a positive 60°–disclination, these stresses effectively relax through formation of a cone structure (Fig. 15d). Insertion of n = 2, 3, 4, 5, and 6 positive 60°–disclinations into a flat graphene sheet allows one to produce topologically and physically distinct cone carbon structures with various curvature characteristics dependent on n (Fig. 16) [39-41]. For instance, a capped carbon nanotube corresponds to the case of n = 6.

Heptagons are negative topological -60°–disclinations in hexagonal crystal lattice of graphene (Fig. 17). Any isolated -60°–disclination (heptagon) in a graphene sheet can be produced by an insertion of a sheet wedge within an angle 60° into a pristine graphene [39-42]. This procedure preserves the hexagonal crystalline order everywhere in the graphene sheet, except for one elementary cell which becomes a heptagon, a topological -60°–disclination (Fig. 17). Such disclinations serve as powerful sources of long-range stresses, and thereby formation of isolated disclinations in flat graphene sheets in most cases is energetically unfavorable. When a negative topological -60°–disclination is inserted into a free-standing graphene sheet, the disclination-induced stresses transform the initially flat sheet into a saddle-like (or Pringle-shaped) carbon structure. Insertion of m ($\geq$ 1) negative 60°–disclinations into a flat graphene sheet allows one to produce topologically distinct saddle-like carbon structures with various curvature characteristics dependent on m (Fig. 18) [39].

The examples discussed above illustrate the role of topological disclinations as curvature carries whose insertion into a mature flat graphene transforms it into curved carbon structures. For geometric reasons, conventional curved carbon nanostructures with the threefold coordination typically contain positive topological 60°–disclinations; see, e.g., [39-42] and references therein. For instance, fullerenes (C_{60}), hyperfullerenes (C_{70}), and hypofullerenes (C_{50}) represent carbon nanostructures each containing 12 topological 60°–disclinations [40], and the difference between these nanostructures is in spatial arrangement of their generic disclinations. Carbon nanocones were produced each containing 1 to 5 positive topological 60°–disclinations, in which case the number of disclinations and their spatial distribution define a nanocone shape [39,40,42]. A pristine open nanotube is free from disclinations; it can be viewed as a graphene sheet rolled into a cylinder. At the same time, for geometric reasons, capped nanotubes definitely contain disclinations.

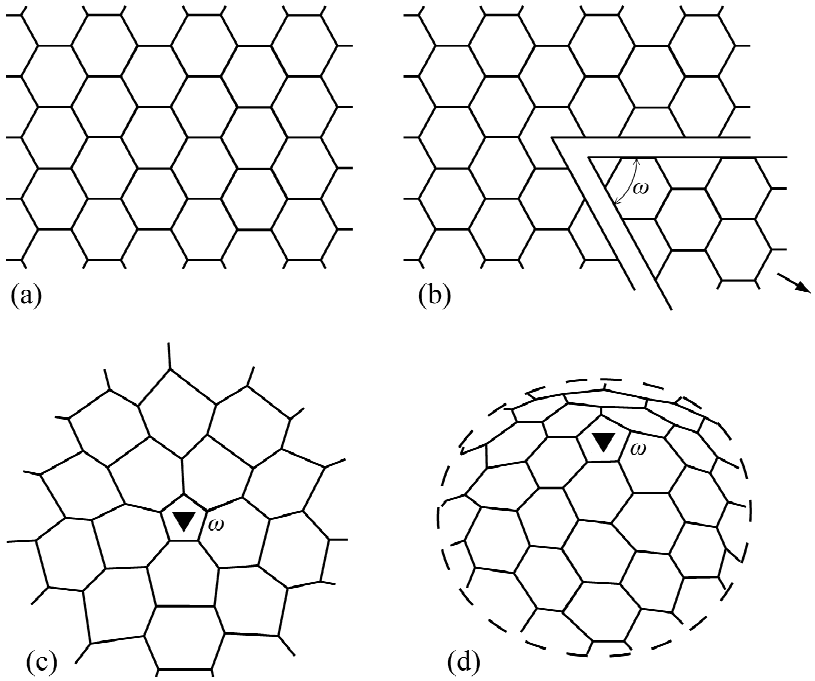

Fig. 15. Formation of a positive topological 60°-disclination in hexagonal crystal lattice of graphene (in spirit of [41]). (a) Initial, ideal state of graphene hexagonal lattice. (b) A 60°-sector is cut and removed from hexagonal lattice. (c) After gluing the cut surfaces, a topological 60°-disclination – pentagon - is formed in hexagonal lattice of plane graphene sheet. The disclination (also shown as small full triangle) creates high in-plane distortions and stresses in plane graphene sheet. (d) Topological 60°-disclination in a free-standing graphene sheet transforms it into a curved cone structure having blunt top.

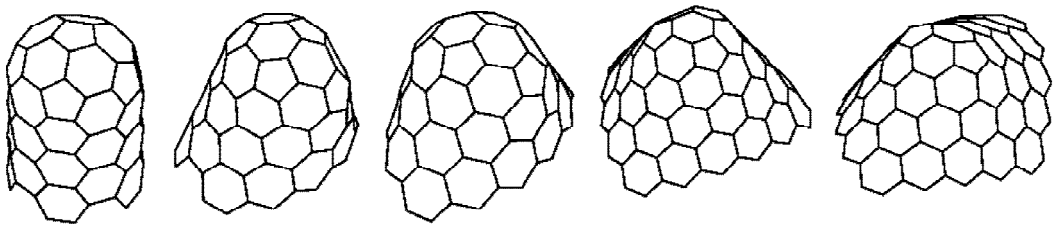

Fig. 16. Graphite monolayer (graphene) structures curved due to positive topological disclinations. Insertion of n = 6, 5, 4, 3, and 2 topological 60°-disclinations (pentagons) in hexagonal crystal lattice of graphite monolayer transform it into cone structures with curvature dependent on n (for details, see [39]). The case of n = 6 corresponds to capped carbon nanotube. Reprinted with permission from [S. Ihara, S. Itoh, K. Akagi, R. Tamura and M. Tsukada, *Physical Review B,* Volume 54 (1996) 14713-14719.], Copyright (1996) by the American Physical Society.

A semi-spherical cap of a carbon nanotube contains 6 topological 60°–disclinations which provide its role as a geometric closure for a nanotube. There are also other examples of curved carbon nanostructures whose curvature characteristics allow one to treat them as topologically distinct carbon allotropes (Fig. 19) [42].

A very interesting special category of carbon nanostructures is represented by hybrid carbon nanostructures defined as nanostructures composed of at least two different carbon allotropes; see, e.g., [43-46]. Their complicated hybrid geometries are associated with specific configurations of topological disclinations. For instance, periodic graphene nanobuds (C_{60} buckyballs) attached to flat graphene were simulated as hybrid carbon nanostructures [43] (Fig. 20). This carbon nanostructure exhibits either semiconductor or semimetallic electronic properties [43], depending on the pattern of carbon atoms or, in other terms, arrangement of topological disclinations within "intermediate" areas between the flat graphene areas and attached C_{60} buckyballs. Another example of hybrid carbon nanostructures is represented by experimentally fabricated nanoscopic peapods; see, e.g., [44,45]. Each peapod is composed of 1D array of

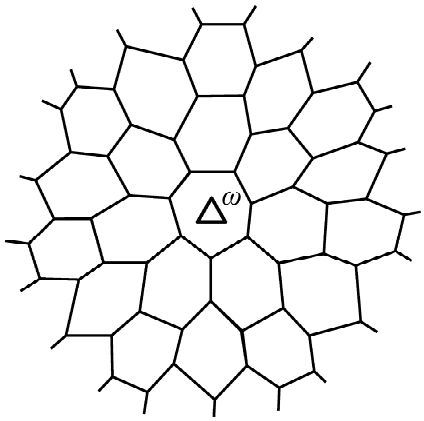

Fig. 17. Negative topological -60°-disclination – heptagon - in hexagonal crystal lattice of graphene. The disclination (also shown as small open triangle) creates high in-plane distortions and stresses in flat graphene sheet.

C_{60} buckyballs/fullerenes nested inside single-walled carbon nanotubes (Fig. 21) [44,45]. In computer simulations [46], it was found that a hybrid peapod consisting of a (10,10) nanotube with internal C_{60} fullerenes is a metal with multicarriers each of which distributes either along the nanotube or on the fullerenes.

The research results presented in this section indicate that curvature and associated configurations of topological disclinations in carbon nanosystems dramatically or even critically influence their structure and properties. In particular, curvature and associated arrangement of topological disclinations in a carbon nanosystem can serve as its definitive structural features, and these features differentiate topologically and physically distinct carbon allotropes such as graphene, fullerenes, cones and others; see, e.g., [2,39-45]. In the context discussed, manipulation with disclination defects in carbon nanosystems is very effective in seeking new carbon materials with novel properties. Up to date, research efforts in this area have been focused on manipulation with topological disclinations with quantized strengths (= $k(60^o)$, where k is an integer) in carbon nanosystems. In next section, we will suggest and present a new strategic approach for generation of new carbon structures with widely (in practice, arbitrarily) ranged geometries. This approach is based on manipulation with GB disclinations hav-

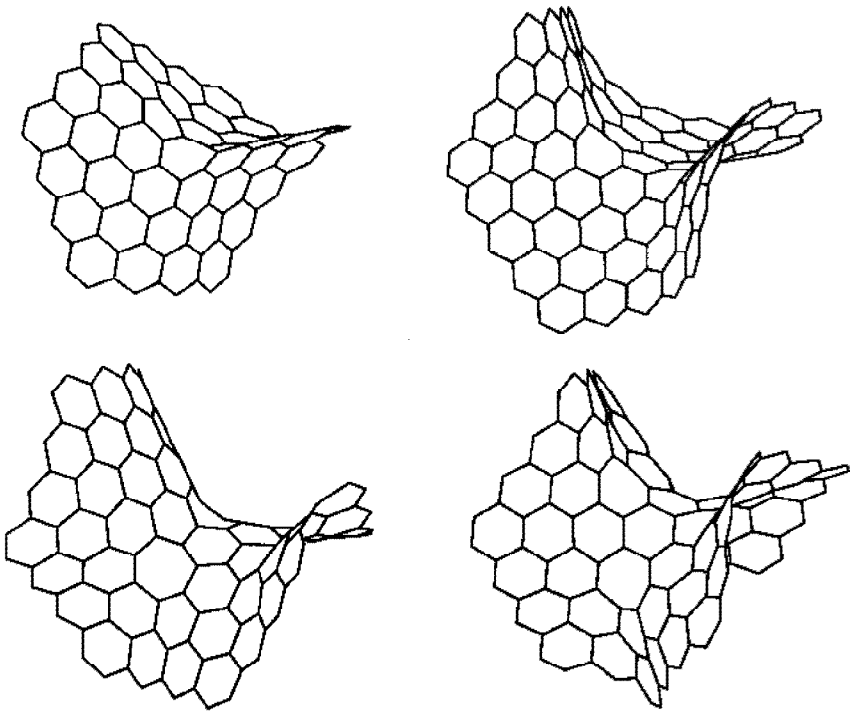

Fig. 18. Graphite monolayer (graphene) structures curved due to negative topological disclinations (heptagons). m = 1, 2, 3, and 4 topological 60°-disclinations (heptagons) in hexagonal crystal lattice of graphite monolayer transform it into saddle-like structures with curvature dependent on m (for details, see [39]). Reprinted with permission from [S. Ihara, S. Itoh, K. Akagi, R. Tamura and M. Tsukada, *Physical Review B,* Volume 54 (1996) 14713-14719.], Copyright (1996) by the American Physical Society.

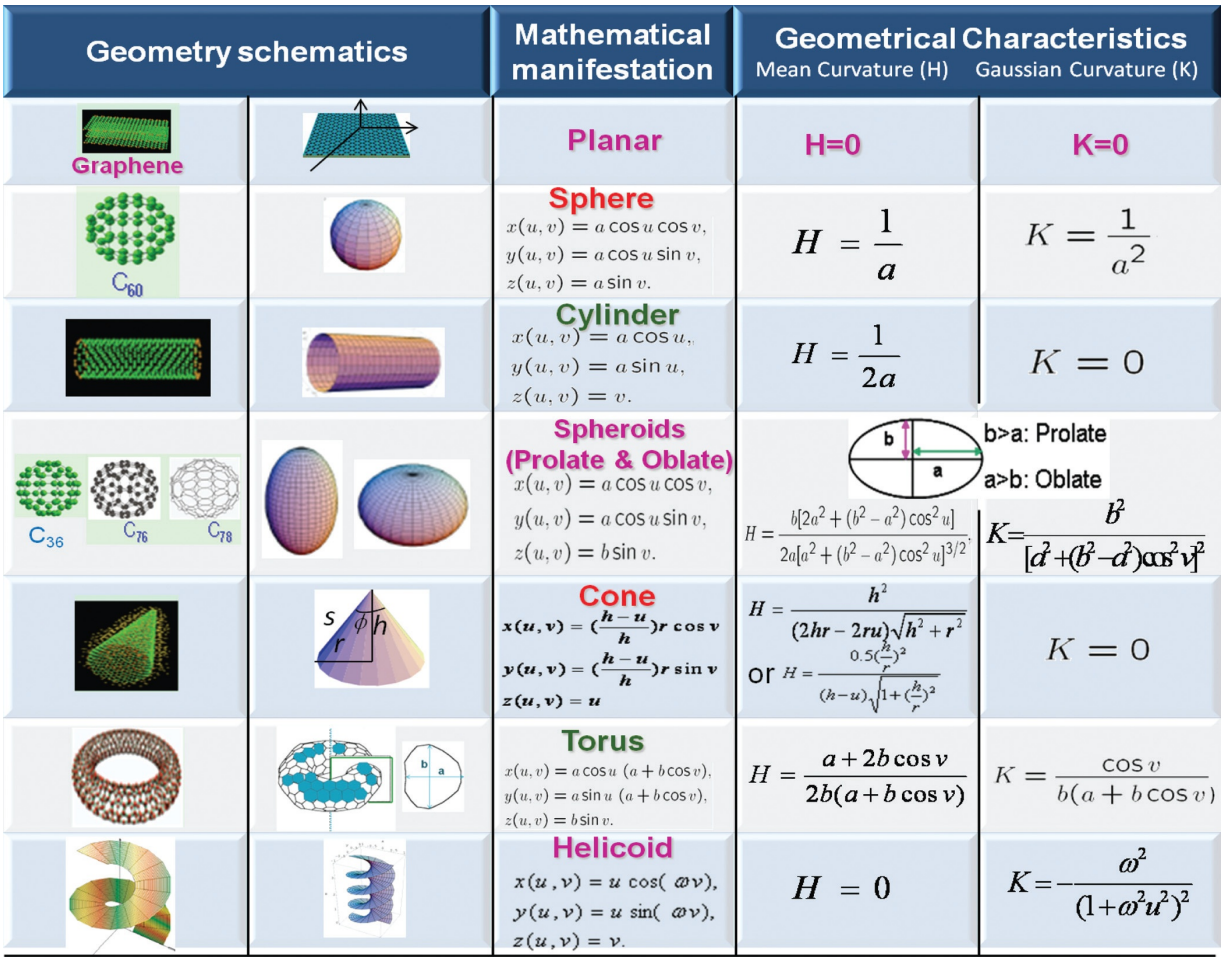

Fig. 19. Summary of schematic geometries and surface parametrization for a range of nanostructured carbon allotropes and corresponding mean and Gaussian curvatures for planar graphene, fullerene (C_{60}), single-walled carbon nanotube, hypo- and hyper fullerenes, nanocone, nanoring/nanotorus and helicoid (for details, see [42]). Reprinted with permission from [S. Gupta and A. Saxena, *Journal of Applied Physics,* Volume 109 (2011) article 074316]. Copyright (2011) American Institute of Physics.

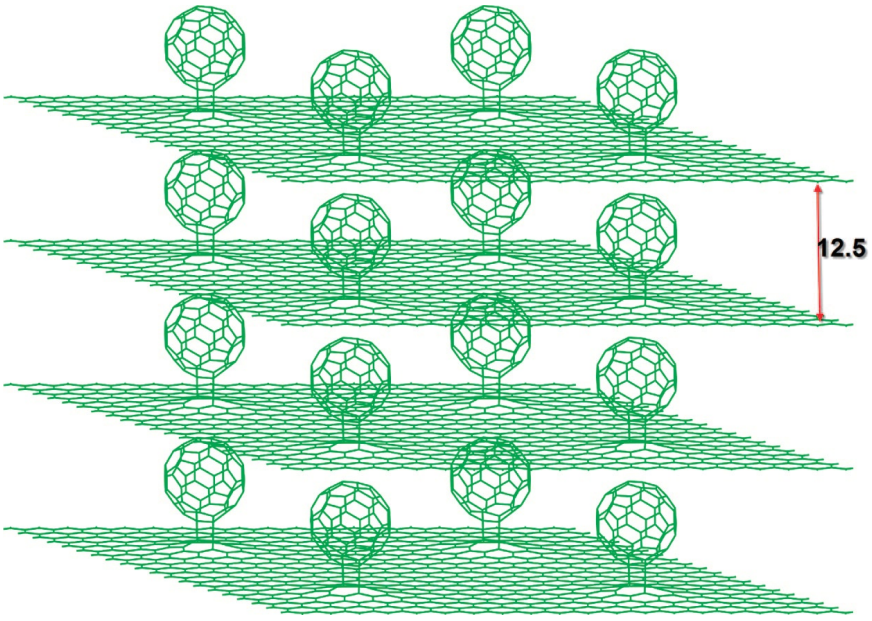

Fig. 20. Optimized multilayer structure of periodic graphene nanobuds. The interlayer distance is about 12,5 A (for details, see [43]). Reprinted with permission from [X. Wu and X.C. Zeng, Periodic graphene nanobuds, *Nano Letters,* Volume 9, No 1 (2009) 250-256]. Copyright (2009) American Chemical Society.

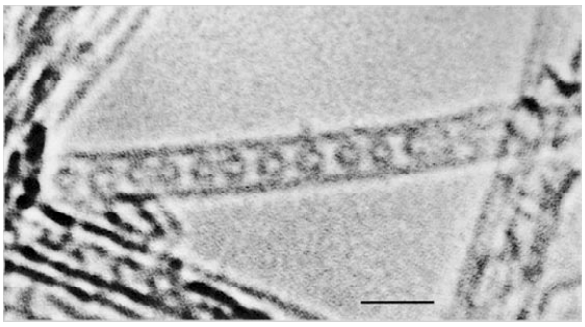

Fig. 21. A single-walled carbon nanotube containing a row of closed carbon shells concentric with the tubule axis. The diameter and and centre-to-centre spacing of the internal shells are consistent with a chain of C_{60} fullerenes. The nanotube is surrounded by a vacuum. Scale bar, 2 nm. (for details, see [44]). Reprinted with permission from [B.W. Smith, M. Monthioux and D.E. Luzzi, *Nature,* Volume 396 (1998) 323-324]. Copyright (1998) by the Macmillan Publishers Limited.

ing non-quantized strengths in graphene (viewed as a mature material) and allows one to generate its curved nano- and polycrystalline specimens that have complicated shapes and can be treated as new carbon allotropes.

6. CURVED NANO- AND POLYCRYSTALLINE GRAPHENE STRUCTURES AS NEW CARBON ALLOTROPES

As it was discussed in previous sections, periodic GBs in free-standing graphene can cause its local buckling (Fig. 6b). The characteristic buckling scale for a periodic GB is close to its period which serves as the screening length for stress fields of GB dislocations, pentagon-heptagon pairs [20]. In real polycrystalline graphene sheets, GBs are not strictly periodic; see, e.g., [11-15]. At the same time, experimentally observed symmetric GBs typically have no large fluctuations of their dislocation densities along the GB lines, in which case they do not create long-range stresses and/or long-range buckling. In doing so, in terms of GB tilt misorientation (carried by GB dislocations), its local value along the GB line is approximately equal to the mean GB misorientation.

In general, however, GBs in graphene, as with other solids, can have step-like variations in the GB misorientation along GB lines. The points where the GB misorientation changes in the abrupt, step-like manner serve as GB disclinations different from previously considered topological disclinations (pentagons, heptagons). More precisely, according to the theory of disclinations in solids [47-49], a wedge disclination at a line GB is the point separating GB fragments with different tilt misorientation angles, whose difference is the disclination strength ω. In general, strengths (ω) of such GB disclinations called also *partial disclinations* can be arbitrary in the range: $-60^o < \omega < 60^o$, in contrast to quantized strengths ($k(60^o)$, where k is an integer) of perfect topological dislocations discussed in previous sections.

Let us consider in detail the geometric aspects concerning formation of symmetric tilt boundary with a positive partial disclination in a flat graphene sheet. For illustration, it is convenient to represent the formation process as the imaginary procedure shown in Fig. 22. More precisely, Fig. 22a presents two graphene bi-crystals with symmetric tilt boundaries. The top bi-crystal has its bottom zigzag free surface E''B''F'' and contains symmetric tilt boundary AB'' characterized by tilt misorientation angle θ_{AB}. The zigzag free surface has two segments, E''B'' and B''F'', tilted by θ_{AB} relative each other. The bottom bi-crystal has its top zigzag free surface E'B'F' and contains symmetric tilt boundary AB' characterized by tilt misorientation angle $\theta_{BC} > \theta_{AB}$. The zigzag free surface has two segments, E'B' and B'F', tilted by θ_{BC} relative each other (Fig. 22a).

Fig. 22b shows the graphene bi-crystals matched at point B coinciding with points B'' and B' of the top and bottom bi-crystals, respectively. Open (free from graphene) wedge-like sectors E''BE' and F''BF' are formed each being characterized by the angle $\omega/2$, where $\omega = \theta_{BC} - \theta_{AB} > 0$. Fig. 22c presents the graphene bi-crystals which are strained in order to fill the aforesaid open sectors, in which case the bi-crystals are matched at their zigzag free surfaces. In doing so, points E'' and E' are matched at point E, points B'' and B' are matched at point B, and points F'' and F' are matched at point F. As a result, large strained bi-crystal is formed which contains symmetric tilt boundary ABC having two segments AB and BC characterized by tilt misorientation angles θ_{AB} and θ_{BC}, respectively, where $\theta_{AB} < \theta_{BC}$ (Fig. 22c). The tilt boundary ABC contains positive partial disclination (small full triangle) characterized by the strength ω and associated with step-like change, $\theta_{BC} - \theta_{AB}$, in its tilt misorientation angle (Fig. 22c). The in-plane strains in the bi-crystal are those created by the partial GB disclination B.

In the case of a free-standing graphene with a positive partial disclination at a GB, disclination-in-

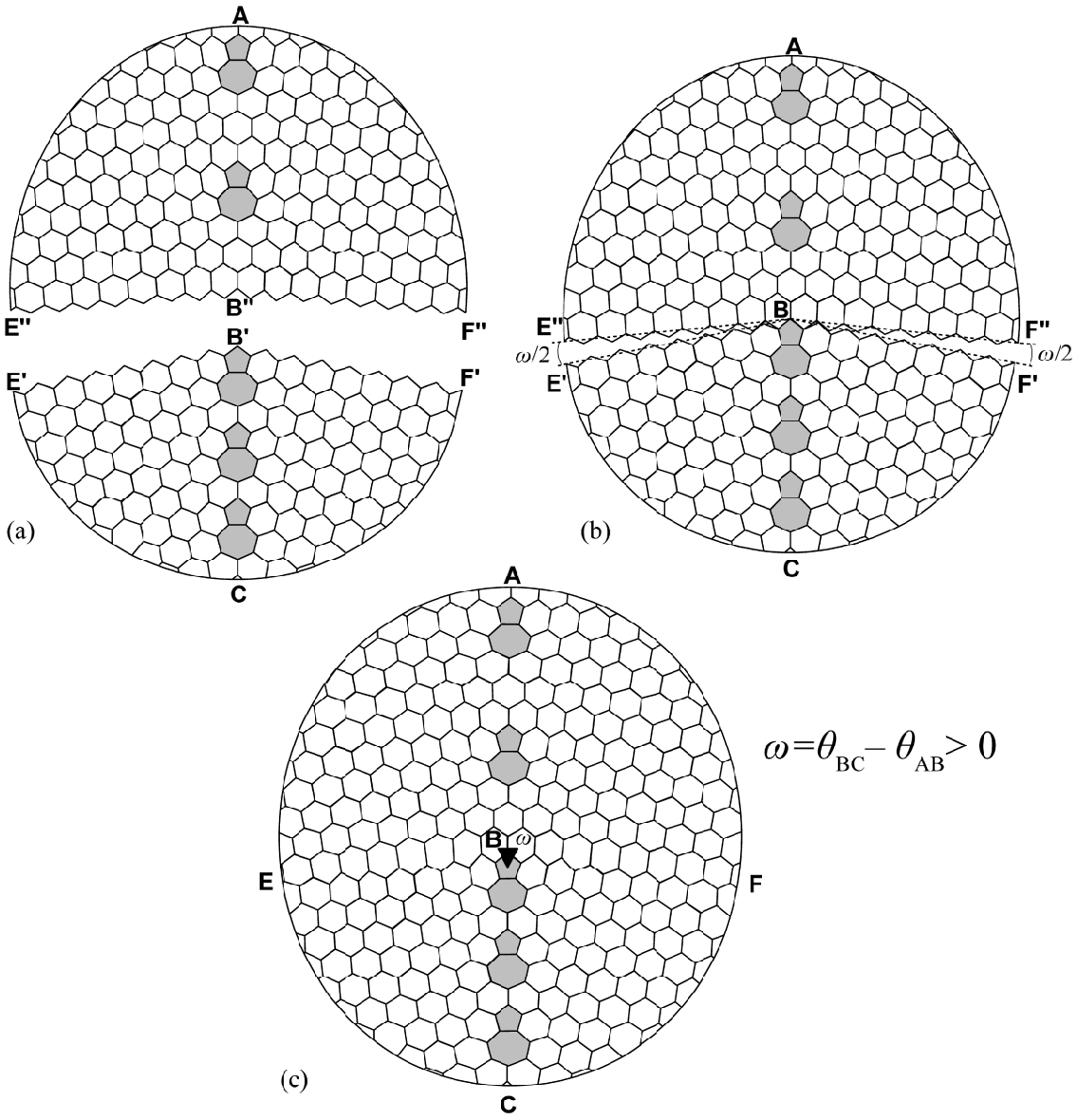

Fig. 22. Formation of symmetric tilt boundary with a positive partial disclination in flat graphene sheet (for details, see the main text). (a) Two separate graphene bi-crystals with symmetric tilt boundaries. (b) The graphene bi-crystals are matched at point B coinciding with points B'' and B' of the top and bottom bi-crystals, respectively. Open wedge-like sectors E''BE' and F''BF' are formed each being characterized by the angle $\omega/2$. (c) The graphene bi-crystals are strained and matched at their zigzag free surfaces. As a result, large strained bi-crystal is formed which contains symmetric tilt boundary ABC having two segments AB and BC characterized by tilt misorientation angles θ_{AB} and θ_{BC}, respectively. The tilt boundary ABC contains positive partial disclination characterized by the strength ω (> 0) associated with step-like change in its tilt misorientation angle at point B.

duced stresses effectively relax through formation of a cone structure like those presented in Figs. 15d and 16. For energy reasons, partial GB disclinations are typically characterized by low values of strength $\omega << 60^o$. In these circumstances, tops of corresponding cone structures of graphene bi-crystals with partial disclinations are rather blunt compared to those presented in Figures 15d and 16. In general, the curvature associated with a partial positive disclination in a cone structure increases with rising the disclination strength ω.

Formation of symmetric tilt boundary with a negative partial disclination in a flat graphene sheet (Fig. 23) can be illustrated in the same imaginary way, as with the negative partial disclination (Fig. 22), but with the proviso that $\theta_{AB} > \theta_{BC}$. That is, the

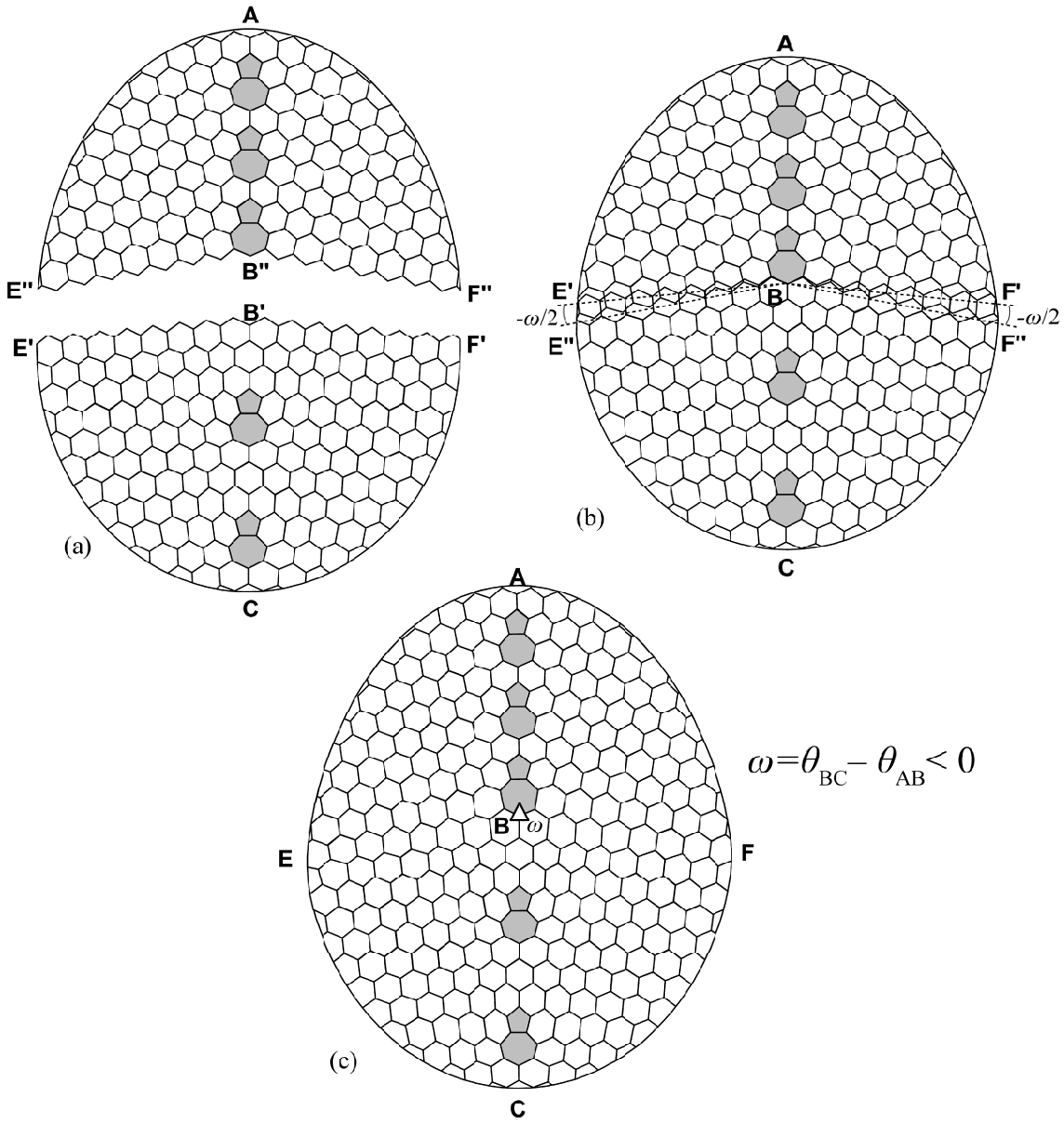

Fig. 23. Formation of symmetric tilt boundary with a negative partial disclination in flat graphene sheet (for details, see the main text). (a) Two separate graphene bi-crystals with symmetric tilt boundaries. (b) The graphene bi-crystals are matched at point B coinciding with points B'' and B' of the top and bottom bi-crystals, respectively. Overlapped wedge-like sectors E''BE' and F''BF' are formed each being characterized by the angle -ω/2. (c) The graphene bi-crystals are strained and matched at their zigzag free surfaces. As a result, large strained bi-crystal is formed which contains symmetric tilt boundary ABC having two segments AB and BC characterized by tilt misorientation angles θ_{AB} and θ_{BC}, respectively. The tilt boundary ABC contains negative partial disclination characterized by the strength ω (<0) associated with step-like change in its tilt misorientation angle.

tilt boundary in the top graphene bi-crystal is characterized by the misorientation angle θ_{AB} exceeding that (θ_{BC}) of the tilt boundary existing in the bottom bi-crystal (Fig. 23). As to details, Fig. 23a shows two graphene bi-crystals with symmetric tilt boundaries. The top bi-crystal has its bottom zigzag free surface E''B''F'' and contains symmetric tilt boundary AB'' characterized by tilt misorientation angle θ_{AB}. The zigzag free surface has two segments, E''B'' and B''F'', tilted by θ_{AB} relative each other. The bottom bi-crystal has its top zigzag free surface E'B'F' and contains symmetric tilt boundary B'C characterized by tilt misorientation angle $\theta_{BC} < \theta_{AB.}$ The zigzag free surface E'B'F' has two segments, E'B' and B'F', tilted by θ_{BC} relative each other (Fig. 23a). Fig. 23b presents the graphene bi-crystals matched at

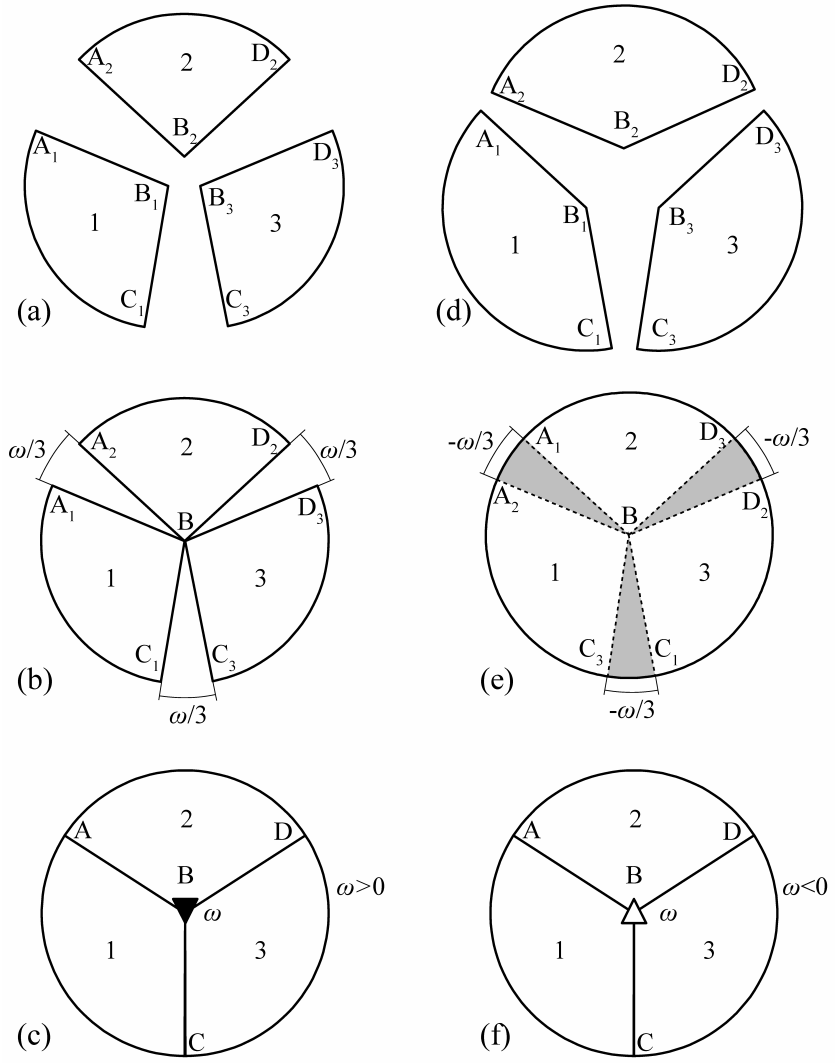

Fig. 24. Formation of partial disclinations at triple junctions of grain boundaries in graphene (schematically). (a-c) Imaginary procedure for formation of a positive disclination at triple junction B in flat graphene sheet. (a) Three separate bi-crystals with symmetric tilt boundaries AB, BC and BD. (b) The three bi-crystals are matched at point B. Open wedge-like sectors are formed each being characterized by the angle ω/3. (c) The three bi-crystals are strained and matched at their free surfaces. As a result, large strained bi-crystal is formed which contains three symmetric tilt boundaries AB, BC and BD that join at the triple junction B. The junction B contains positive partial disclination characterized by the strength ω (> 0) associated with the angle gap being the sum of the misorientation angles of the tilt boundaries AB, BC and BD. (d-f) Imaginary procedure for formation of a negative disclination at triple junction B in flat graphene sheet. (d) Three separate bi-crystals with symmetric tilt boundaries AB, BC and BD. (e) The three bi-crystals are matched at point B. Overlapped wedge-like sectors are formed each being characterized by the angle -ω/3. (f) The three bi-crystals are strained and matched at their free surfaces. As a result, large strained bi-crystal is formed which contains symmetric three tilt boundaries AB, BC and BD that join at the triple junction B. The junction B contains negative partial disclination characterized by the strength ω (< 0) associated with the angle gap being the sum of the misorientation angles of the tilt boundaries AB, BC and BD.

point B coinciding with points B'' and B' of the top and bottom bi-crystals, respectively. Overlapped wedge-like sectors E'BE'' and F'BF'' (sectors containing overlapped parts of the top and bottom bi-crystals) are shown each being characterized by the angle -ω/2, where $\omega = \theta_{BC} - \theta_{AB} < 0$ (Fig. 23b). Fig. 23c presents the graphene bi-crystals which are strained in order to be matched at their zigzag

free surfaces. In doing so, points E'' and E' are matched at point E, points B'' and B' are matched at point B, and points F'' and F' are matched at point F. As a result, a large strained bi-crystal is formed which contains symmetric tilt boundary ABC having two segments AB and BC characterized by tilt misorientation angles θ_{AB} and θ_{BC}, respectively, where $\theta_{AB} > \theta_{BC}$ (Fig. 23c). The tilt boundary CBA contains negative partial disclination (small open triangle) characterized by the strength $\omega < 0$ and associated with step-like change, $\theta_{BC} - \theta_{AB} < 0$, in its tilt misorientation angle (Fig. 23c).

The partial negative disclination B at the GB ABC creates in-plane strains in the flat bi-crystal (Fig. 23c). In the situation with a free-standing graphene sheet containing a negative partial disclination at a GB, the disclination-induced stresses transform the sheet into a saddle-like carbon structure like those presented in Fig. 18.

Also, partial disclinations can exist at triple junctions of GBs in graphene (Fig. 24). A disclination is present at a triple junction of tilt boundaries, if the sum of tilt misorientation angles of these boundaries is non-zero (Fig. 24). By analogy with triple junction disclinations in 3D solids [47-49], the non-zero sum (angle gap) at a triple junction in graphene serves as the disclination strength.

Figs. 24a-24c schematically shows geometric aspects concerning the formation of a positive disclination at the triple junction B in a flat graphene sheet. The formation geometry is very similar to that for a negative disclination at a GB (Fig. 22). In the situation with a free-standing graphene sheet containing a positive partial disclination at a triple junction of GBs, the disclination-induced stresses transform the sheet into a cone structure like those presented in Figs. 15d and 16.

Figs. 24d-24f schematically shows geometric aspects concerning the formation of a negative disclination at the triple junction B in a flat graphene sheet. The formation geometry is very similar to that for a negative disclination at a GB (Fig. 23). In the situation with a free-standing graphene sheet containing a negative partial disclination at a triple junction of GBs, the disclination-induced stresses transform the sheet into a saddle-like carbon structure like those presented in Fig. 18.

It is very important to note that, from a geometric viewpoint, the disclination strengths (ω) of partial disclinations at GBs and triple junctions (Figs. 22, 23 and 24) are not quantized; they are valued in the range: $-60^o < \omega < 60^o$. For instance, the ω magnitude can be very small (~ $1\text{-}5^o$), and this is reasonable from energy consideration. Arbitrary values of strengths characterizing partial disclinations at GBs and their triple junctions (Figs. 22, 23 and 24) are contrasted to strictly quantized strengths ($k(60^o)$, where k is an integer) of perfect topological disclinations (Figs. 15 and 17) - pentagons, heptagons, octagons, etc. - in graphene lattice. This difference in geometry between partial and topological disclinations provides preference of partial disclinations as more flexible carriers of curvature in construction of carbon nanostructures, compared to topological disclinations. That is, it is more effective and variable to exploit partial disclinations (instead of topological disclinations) as structural elements of curved carbon nanostructures.

In general, partial disclinations with non-quantized strengths are rather typical defects in various solids. For instance, following numerous experimental data, theoretical examinations and computer simulations, partial disclinations are often formed at GBs and triple junctions in nanocrystalline and polycrystalline bulk materials, thin films and nanowires, where they effectively contribute to the properties of these 3D solids; see, e.g., [47-56].

With arbitrary values of strengths characterizing partial disclinations at GBs and their triple junctions (Figs. 22, 23 and 24), GB engineering through arrangement of partial disclinations in mature free-standing graphene sheets represents a very effective approach to product new curved carbon with novel properties. In particular, one can generate curved carbon structures having, in practice, arbitrary shapes (see, e.g., Fig. 25), and these structures are capable of exhibiting desired functional and mechanical properties depending on their controlled structural geometry. The suggested design of curved polycrystalline and nanocrystalline graphene with GBs containing partial disclinations potentially allows one to produce a wide variety of new carbon allotropes with outstanding properties. In doing so, combined effects of GBs and curvature can generate absolutely novel properties of such carbon allotropies.

7. CONCLUDING REMARKS

Thus, GBs – line defects separating grains (domains/crystallites) with different lattice orientations - represent typical defects in graphene sheets. In particular, their presence is, by practice, inevitable in large-area graphene sheets which are of utmost interest for potential technological applications. Following experimental data, theoretical examinations and computer simulations discussed in this review, dominating GB structures in graphene are

Fig. 25. An imaginary "Venus of Milos" carbon allotrope has 3D landscape corresponding to the famous sculpture. The carbon allotrope can be fabricated through special grain boundary engineering - generation of grain boundaries with partial disclinations - in a mature polycrystalline graphene. Grain boundary network in the "Venus of Milos" carbon allotrope is schematically shown as a network of solid lines. A magnified inset shows a grain boundary fragment containing a partial positive disclination.

those consisting of topological dislocations, that is, pentagon-heptagon pairs in hexagonal graphene lattice (Figs. 3d and 3e, 4, 5, 7-9). Experimentally observed GBs in graphene sheets represent topological dislocation walls which are curved and show no strict periodicity [11,13] (Figs. 4 and 7). In a partial case, GB loops can be formed in graphene [14] (Fig. 8). Such GB loops with simplest geometry were experimentally observed as flower defects [14] (Fig. 9).

GBs in a free-standing graphene typically cause its local buckling [19,20] (Fig. 6b). In particular, arrangement of topological dislocations (pentagon-heptagon pairs) into a periodic line GB gives rise to formation of linear bridges in a free-standing graphene sheet [20] (Fig. 6b). If a graphene monolayer with a 3D landscape created by pentagon-heptagon pairs is attached to a substrate, the landscape is partially flattened owing to the interaction between atoms of the graphene sheet and the substrate [20] (Fig. 6c).

In parallel with GBs consisting of pentagon-heptagon pairs (topological dislocations) and distorted hexagons in graphene, preserving the threefold coordination of the carbon atoms, there are also examples of GBs that contain dangling bonds violating the threefold coordination [25]. Another experimentally observed example of non-conventional GB configurations is represented by anomalously wide GBs with a disordered structure in a few-layer graphene [12] (Fig. 12). In Fig. 12, such a GB region is shown which separates large misoriented grains, has the width of ~ 50 nm and contains randomly oriented parallel 1D features with a periodicity of ~ 4 nm.

GB ensembles in graphene are characterized by GB misorientation distributions which show some specific features. First, in a polycrystalline graphene grown on Cu, there is the dominance of high-angle boundaries having the misorientation angle in the range from 10^{o} to 30^{o} [25]. In contrast, in free-standing graphene sheets, GB misorientation angles tend

to have more populations around 0^o and 30^o than middle-range angles [11,13] (Figs. 10 and 11).

GBs in graphene specimens are capable of significantly or even crucially influencing their outstanding mechanical and transport properties. In particular, following experimental data [11], the failure strength of free-standing polycrystalline graphene under concentrated mechanical load dramatically degrades compared to single-crystal graphene areas. In computer simulations [32], it was found that graphene sheets containing high-angle GBs with dense dislocation structures have strength values exceeding those of graphene sheets containing low-angle GBs with low-density dislocation structures (Fig. 13).

Following the experimental data [11,15], the transport properties of graphene degrade due to GBs, but the measured resistance of GBs is not dramatically different from that of graphene free from GBs. Yazyev and Louie [36] theoretically revealed the two distinct transport behaviors - high transparency and perfect reflection of charge carriers over large energy ranges (up to ~1 eV) - of periodic GBs, depending on their structural and geometric features. These results are of crucial interest for potential applications of polycrystalline graphene in electronics [36,37].

Also, we briefly reviewed the concept that curvature and associated disclination configurations in carbon nanosystems serve as their critical structural characteristics, and these characteristics differentiate topologically and physically distinct carbon allotropes such as graphene, nanotubes, fullerenes, cones and others; see, e.g., [2,39-45]. With this concept, it is concluded that manipulation with the disclination defects in carbon nanosystems is very effective in seeking new carbon materials with novel properties.

In Section 6, a new approach for generation of new carbon structures with various (in practice, arbitrary) geometries has been suggested. Within this approach, GB engineering through formation of partial disclinations in graphene is supposed to be a very promising and effective method for fabrication of curved nano- and polycrystalline graphene specimens that have complicated shapes and can be treated as new carbon allotropes.

In general, studies of GBs in graphene are in their infancy. Therefore, there are many unsolved problems in science and technology of polycrystalline graphene. In this context, in the conclusion of this paper, let us outline important unsolved problems in this area. They are briefly as follows:

(A) Fabrication of polycrystalline and nanocrystalline graphene specimens - monolayers attached to substrates as well as free-standing sheets - with controlled geometric and structural parameters of GBs.

(B) Unambiguous experimental identification, computer modeling and theoretical description of the effects of GBs on the outstanding physical, mechanical and chemical properties of conventional polycrystalline and nanocrystalline graphene with approximately flat geometry. In doing this research, it is important to distinguish the effects of GBs on the properties of graphene within the following four categories: (i) the effects of GB dislocation cores (pentagon-heptagon pairs); (ii) the effects associated with orientation mismatch between grains/crystallites matched at GBs; (iii) the effects of in-plane strains induced by GBs; and (iv) the effects of local buckling induced by GBs.

(C) With (A) and (B) used as an input, fabrication of polycrystalline and nanocrystalline flat graphene specimens with physical, mechanical and chemical properties tuned and controlled by GB engineering in these specimens.

(D) Search for and fabrication of new carbon nanostructures/allotropes as curved polycrystalline and nanocrystalline graphene specimens with GBs containing partial disclinations, carriers of a non-zero curvature.

(E) Experimental identification, computer modeling and theoretical description of the effects of GBs on the physical, mechanical and chemical properties of curved polycrystalline and nanocrystalline graphene with GBs containing partial disclinations.

(F) With (D) and (E) used as an input, fabrication of curved polycrystalline and nanocrystalline graphene specimens (containing disclinated GBs) with physical, mechanical and chemical properties tuned and controlled by the engineering of disclinated GBs in these specimens.

(G) Search for and fabrication of new hybrid carbon nanostructures - nanostructures composed of at least two different carbon allotropes – through the engineering of disclinated GBs in mature graphene sheets.

Success in treatment of these important unresolved questions will make a large impact on fundamental science of graphene and open new intriguing perspectives in fabrication of graphene and new curved carbon nanostructures having GB-controlled properties for a wide range of technological applications.

ACKNOWLEDGEMENTS

This work was supported in part by the Ministry of Education and Science of the Russian Federation (Contract 14.740.11.0353) and the Russian Foundation of Basic Research (grant 12-01-00291-a).

REFERENCES

[1] K.S. Novoselov, A.K. Geim, S.V. Morozov, D. Jiang, Y. Zhang, S.V. Dubonos, I.V. Grigorieva and A.A. Firsov // *Science* **306** (2004) 666.

[2] A.K. Geim and K.S. Novoselov // *Nature Mater*. **6** (2007) 183.

[3] A.K. Geim // *Science* **324** (2009) 1530.

[4] A.H. Castro Nero, F. Guinea, N.M.R. Peres, K.S. Novoselov and A.K. Geim // *Rev. Mod. Phys*. **81** (2009) 109.

[5] F. Molitor, J. Guttinger, C. Stampfer, S. Droscher, A. Jacobson, T. Ihn and K. Ensslin // *J. Phys.: Condens. Matter* **23** (2011) 1.

[6] C. Lee, X. Wei, J.W. Kysar and J. Hone // *Science* **321** (2008) 385.

[7] K.V. Emtsev, A. Bostwick, K. Horn, J. Jobst, G.L. Kellogg. L. Ley, J.L. McChesney, T. Ohta, S.A. Reshanov, J. Rohl, E. Rotenberg, A. Schmid, D. Waldmann, H.B. Weber and T. Seyller // *Nature Mater*. **8** (2009) 203.

[8] A. Reina, X. Jia, J. Ho, D. Hezich, H. Son, V. Bulovic, M.S. Dresselhaus and J. Kong // *Nano Lett*. **9** (2009) 30.

[9] K.S. Kim, Y. Zhao, H. Jang, S.Y. Lee, J.M. Kim, K.S. Kim, J.-H. Ahn, P. Kim, J.-Y. Choi and B.H. Hong // *Nature* **457** (2009) 706.

[10] X. Li, W. Cai, J. An, S. Kim, J. Nah, D. Yang, R. Piner, A. Velamakanni, I. Jung, E. Tutuc, S.K. Banerjee, L. Colombo and R.S. Ruoff // *Science* **324** (2009) 1312.

[11] P. Y. Huang, C.S. Ruiz-Vargas, A. M. van der Zande, W.S. Whitney, M.P. Levendorf, J.W. Kevek, S. Garg, J.S. Alden, C.J. Hustedt, Y. Zhu, J. Park, P.L. McEuen and D.A. Muller // *Nature* **469** (2011) 389.

[12] L.B. Biedermann, M.L. Bolen, M.A. Capano, D. Zemlyanov and R.G. Reifenberger // *Phys. Rev. B* **79** (2009) 125411.

[13] K. Kim, Z. Lee, W. Regan, C. Kisielowski, M.F. Gommie and A. Zettl // *ACS Nano* **5** (2011) 2142.

[14] E. Cockayne, G.M. Rutter, N.P. Guisinger, J.N. Crain, P.N. First and J.A. Stroscio // *Phys. Rev. B* **83** (2011) 195425

[15] Q. Yu, L.A. Jauregui, W. Wu, R. Colby, J. Tian, Z. Su, H. Cao, Z. Liu, D. Pandey, D. Wei, T.F. Chung, P. Peng, N.P. Guisinger, E.A. Stach, J. Bao, S.-S. Pei and Y.P. Chen // *Nature Mat*. **10** (2011) 443

[16] J.C. Meyer, C. Kisielowski, R. Erni, M.D. Rossell, M.F. Gommie and A. Zettl, *Nano Lett.* **8** (2008) 3582.

[17] A. Hashimoto, K. Suenaga, A. Gloter, K. Urita and S. Ijima // *Nature* **430** (2004) 870.

[18] C.O. Girit, J.C. Meyer, R. Erni, M.D. Rossell, C. Kisielowski, L. Yang, C.-H. Park, M.F. Gommie, M.L. Cohen, S. Louie and A. Zettl // *Science* **323** (2009) 1705.

[19] O.V. Yazyev and S. Louie // *Phys. Rev. B* **81** (2010) 195420.

[20] Y. Liu and B.I. Yakobson // *Nano Lett*. **10** (2011) 2178.

[21] P. Simonis, C. Goffaux, P.A. Thilly, L.P. Biro, Ph. Lambin and V. Meunier // *Surf. Sci.* **511** (2002) 319.

[22] W.T. Read and Shockley // *Phys. Rev*. **78** (1950) 275.

[23] J.P. Hirth and J. Lothe, *Theory of Dislocations* (Wiley, New York, 1982).

[24] J. Coraux, A.T. N'Diaye, C. Busse and T. Michely // *Nano Lett*. **8** (2008) 565.

[25] J. An, E. Voelkl, J. Suk, X. Li, C.W. Magnuson, L. Fu, P. Tiemeijer, M. Bischoff, B. Freitag, E. Popova and R.S. Ruoff // *ACS Nano* **5** (2011) 2433.

[26] A.P. Sutton and R.W. Balluffi, *Interfaces in Crystalline Materials* (Oxford Science Publ., Oxford, 1996).

[27] C.C. Koch, I.A. Ovid'ko, S. Seal and S. Veprek, *Structural Nanocrystalline Materials: Fundamentals and Applications* (Cambridge University Press, Cambridge, 2007).

[28] H. Hilgenkamp and J. Mannhart // *Rev. Mod. Phys.* **74** (2002) 485.

[29] I.A. Ovid'ko // *Int. Mater Rev.* **50** (2005) 65.

[30] C.S. Pande and K.P. Cooper // *Progr. Mater. Sci.* **54** (2009) 689.

[31] I.A. Ovid'ko and A.G. Sheinerman // *Rev. Adv. Mater. Sci*. **29** (2011) 105.

[32] R. Grantab, V.B. Shenoy and R.S. Ruoff // *Science* **330** (2010) 946.

[33] J. da Silva Araujo and R.W. Nunes // *Phys. Rev. B* **81** (2010) 073408
[34] A. Cortijo and M. A. H. Vozmediano // Europhys. Lett. 77 (2007) 47002.
[35] J. Smotlacha, R. Pincak and M. Pudlak // Eur. Phys. J. B 84 (2011) 255]
[36] O.V. Yazyev and S. Louie // *Nature Mater*. **9** (2010) 806.
[37] P. Kim // *Nature Mater*. **9** (2010) 792
[38] N. Levy, S.A. Burke, K.L. Meaker, M. Panlasigui, A. Zettl, F. Guinea, A.H. Castro Neto and M.F. Grommie // *Science* **329** (2010) 544
[39] S. Ihara, S. Itoh, K. Akagi, R. Tamura and M. Tsukada // *Phys. Rev. B* **54** (1996) 14713.
[40] A. Krishnan, E. Dujardin, M.M.J. Treacy, J. Hugdahl, S. Lynum and T.W. Ebbesen // *Nature* **388** (1997) 451.
[41] A.L. Kolesnikova and A.E. Romanov // *Phys. Sol. State* **40** (1998) 1075.
[42] S. Gupta and A. Saxena // *J. Appl, Phys*. **109** (2011) 074316.
[43] X. Wu and X.C. Zeng // *Nano Lett*. **9** (2009) 250.
[44] B.W. Smith, M. Monthioux and D.E. Luzzi // *Nature* **396** (1998) 323.
[45] D.J. Hornbaker, S.-J. Kahng, S. Misra, B.W. Smith, A.T. Johnson, E.J. Mele, D.E. Luzzi and A. Yazdani // *Science* **295** (2002) 828.
[46] S. Okada, S. Saito and A. Oshiyama // *Phys. Rev. Lett*. **86** (2001) 3835.
[47] A.E. Romanov and V.I. Vladimirov, In: *Dislocations in Solids*, edited by F.R.N. Nabarro, North-Holland Publ. Co., Amsterdam (1992). Vol. 9, pp. 191–302.
[48] M.Yu. Gutkin and I.A. Ovid'ko, *Plastic Deformation in Nanocrystalline Materials,* (Springer, Berlin, New York, etc., 2004).
[49] M. Kleman and J. Friedel // *Rev. Mod. Phys.* **80** (2008) 61.
[50] P. Klimanek, V. Klemm, A.E. Romanov and M. Seefeldt // *Adv. Eng. Mater*. **3** (2001) 877.
[51] I.A. Ovid'ko // *J. Phys.: Condens. Matter* **13** (2001) L97.
[52] I.A. Ovid'ko // *Science* **295** (2002) 2386.
[53] M. Murayama, J.M. Howe, H. Hidaka and S. Takaki // *Science* **295** (2002) 2433.
[54] K. Zhou, A.A. Nazarov and M.S. Wu // *Phys. Rev. Lett*. **98** (2007) 035501.
[55] I.A. Ovid'ko and A.G. Sheinerman // *Appl. Phys. Lett*. **90** (2007) 171927; *Acta Mater*. **57** (2009) 2217.
[56] N.F. Morozov, I.A. Ovid'ko and N.V. Skiba // *Rev. Adv. Mater. Sci*. **29** (2011) 180.
[57] S.V. Bobylev, N.F. Morozov and I.A. Ovid'ko // *Phys. Rev. Lett*. **105** (2010) 055504; *Phys. Rev. B* **84** (2011) 094103.

Readers may view, browse, and/or download material - figures 3, 8, 9, 12, 16 and 18 reprinted with permission from Physical Review B papers published by the American Physical Society - for temporary copying purposes only, provided these uses are for noncommercial personal purposes. Except as provided by law, this material may not be further reproduced, distributed, transmitted, modified, adopted, performed, displayed, published, or sold in whole or part, without prior written permission from the American Physical Society.